A HOMOGENISED MODEL FOR A REACTIVE FILTER*

KRISTIAN B. KIRADJIEV†, CHRISTOPHER J. W. BREWARD†, IAN M. GRIFFITHS†, AND DONALD W. SCHWENDEMAN‡

Abstract. Many chemical filters contain reactive components where harmful substances are removed or transformed. In this paper, we derive a homogenised model for a flue-gas filter that converts sulphur dioxide into liquid sulphuric acid. We consider a microscale domain, focused on a single catalytic pellet, and homogenise over both the gaseous and the liquid phase to obtain macroscale equations for the concentration of sulphur dioxide and the thickness of the liquid sulphuric acid layer that grows around the pellets. We explore two interesting limits of the homogenised model, in which the reaction rate at the pellet surface is small, and where the mass transfer across the gas–liquid interface is small, respectively. We then couple the macroscale equations to an equation governing the external gas flow through the filter. We solve the resulting model and consider asymptotic reductions based on the filter geometry. We consider two distinguished limits and, for one of them, obtain an explicit solution for the sulphur dioxide concentration and the void fraction in the filter. We vary parameters such as the gas speed and establish the operating regimes for effective cleansing of flue gas.

Key words. homogenisation, reactive porous media, filtration, flue gas, sulphur dioxide

AMS subject classifications. 35B27, 35B40, 35K57, 76S05, 80A30

1. Introduction.

In the drive to protect the environment, reducing the concentrations of harmful chemicals that are released into the atmosphere has become a priority for industry. One key example is the removal of sulphur dioxide, which is formed in vast quantities in industrial processes and power plants as a by-product of processing of raw materials such as crude oil and various ores [17, 38, 43], from flue (exhaust) gas. Sulphur dioxide is a highly toxic gas that can cause acid rain and is linked to respiratory illnesses [7, 43]. In order to decrease its concentration in flue gas, filtering procedures such as "gas scrubbing" (both wet and dry [15, 21, 35]), membrane gas absorption [25], and packed-bed absorption [23] are often used. However, most existing methods require high input power and a specifically suited operation site. In addition, they produce a large amount of waste, such as gypsum containing impurities [38]. This can be quite expensive and time-consuming for companies to implement.

In this paper, we derive and analyse a mathematical model for a more desirable and cost-effective chemical filter, designed by W. L. Gore and Associates, that purifies flue gas and, in particular, removes sulphur dioxide by turning it into liquid sulphuric acid. The filtering device under consideration is made of stackable modules, each of which consists of a series of open channels made of folded porous sheets that contain multiple microscopic catalytic pellets that are held together by a network of fibres (referred to as a sorbent–polymer composite) [26]. Flue gas flows from one end of the filter to the other through the channels and diffuses into the sheets. When sulphur dioxide, oxygen and water-vapour molecules come into contact with the surface of these pellets, they react to form liquid sulphuric acid (see Figure 1 for an illustration of the filtering device and a schematic of the filtration process). In reality, there are

*Submitted to the editors DATE.

Funding: This publication is based on work partially supported by the EPSRC Centre For Doctoral Training in Industrially Focused Mathematical Modelling (EP/L015803/1) in collaboration with W. L. Gore and Associates.

†University of Oxford, Oxford, UK (kiradjiev@maths.ox.ac.uk, https://www.maths.ox.ac.uk/people/kristian.kiradjiev, breward@maths.ox.ac.uk, ian.griffiths@maths.ox.ac.uk).

‡Rensselaer Polytechnic Institute, Troy, NY, USA (schwed@rpi.edu).

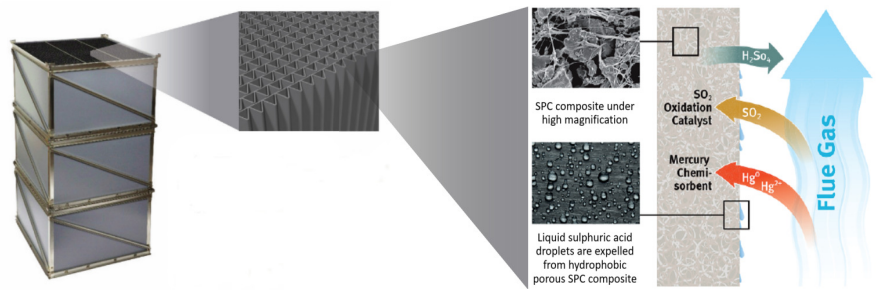

FIGURE 1. *Three modules of the filter device and a schematic of the filtration process (from [26]).*

multiple intermediate reactions that take place in the filter medium (see, for example, [20, 33]) before acid is produced, but for simplicity these can be summarised by the following single effective chemical reaction

$$2\,SO_{2(\star)} + 2\,H_2O_{(\star)} + O_{2(\star)} \xrightarrow[k]{\text{carbon catalyst}} 2\,H_2SO_{4(l)}, \tag{1.1}$$

where k is the overall reaction rate taking into account all intermediate steps, and $(\star)$ denotes gaseous state (g) initially, before a liquid layer has formed around the catalytic pellet, and aqueous solution (aq) afterwards. This method of sulphur dioxide removal is less costly in terms of maintenance, is easy to install in a factory, does not generate toxic waste, and produces sulphuric acid "for free" which can be easily stored or used for other purposes, and also acts as a natural cleanser of the filter by removing contaminant particles such as dust [26]. However, as the chemical reaction proceeds within the filter sheets, liquid sulphuric acid accumulates in the void space (that is, the volume that is neither solid nor liquid) between the catalytic pellets and dramatically reduces the amount of sulphur dioxide that can be processed by the device, resulting in a drop in the device efficiency over time. Our aim is to understand the dynamics of the liquid and gas transport in the filter sheets during operation in order to gain insight into the details of the efficiency reduction and to be able to advise on an optimal operating regime.

Although various models exist for other purification methods, including gas scrubbing [15, 21, 24, 32] and absorption [9, 39], reactive-pellet chemical filters that involve a phase change of the contaminant are less well studied. Mochida *et al.* [33] study the removal of sulphur dioxide using activated carbon fibres, again producing sulphuric acid. They develop a power-law model to describe the steady-state concentration of sulphur dioxide at the outlet of the device and find that this concentration is proportional to the weight of the catalyst and to a specific power of the starting concentrations of sulphur dioxide, oxygen, and water vapour. In addition, they assert that the rate-limiting step of the reaction is the dissociation of sulphuric acid into an aqueous solution around the carbon. Similar findings appear in Gaur *et al.* [19], where they first develop a detailed kinetic model and then describe the evolution of the gas concentration. They observe that increasing the inlet sulphur dioxide concentration or decreasing the oxygen and water-vapour concentrations increases the outlet concentration. In neither of these models is the evolution of the liquid sulphuric acid explicitly modelled. Furthermore, in the second model the functional form of the concentration of sulphur dioxide in the fibre pores is assumed, and, in addition, the governing equations make use of an effective take-up rate of sulphur dioxide and are

derived from a simple averaging over the pore domain. A summary of the time it takes for the effluent gas concentration to reach a specific pre-determined value in gas removal using catalysts for various models can be found in [49].

One approach to studying the physics and chemistry of these reactive filters would be to solve a detailed model of the microscale throughout the filter using an appropriate software package. However, this would be computationally infeasible for realistic filter sizes. Instead, we will appeal to homogenisation theory (see, for example, [4, 8, 22]) and upscale the equations that hold on the scale of a catalytic pellet to obtain an averaged model on the macroscale that captures all the microscale physics.

Relevant physical situations that can be modelled using reaction–diffusion processes occurring at the microscale in a porous medium include solute transport [1, 2, 11, 16, 18, 31, 37, 40, 45], nutrient transport [10, 14], filtration [12, 13], decontamination [29], and dissolution and growth of materials, such as crystals [5, 6, 41, 46, 47] and biofilms [27, 36, 44, 48]. In these situations, the microscale models often describe conservation of mass and momentum of the phases involved, coupled with advection–diffusion equations describing the transport of chemicals, and surface or bulk reactions that contribute to the evolution. These microscale problems can be homogenised by performing a multiple-scales analysis, and the resulting macroscale equations often have a reaction–diffusion–advection form. For example, Conca *et al.* [11] consider the problem of homogenising a flow around reactive solid grains, and they derive upscaled equations for the cases when the reaction happens on the surface of the grains or within the grains, and the resulting macroscale equations are of reaction–diffusion form. A homogenised model for bacterial nutrient uptake in a bioreactor is derived in Dalwadi *et al.* [14]. The reactor is modelled as a fluid medium with dissolved nutrients that diffuse around, and into, a periodic array of spherical bacteria, where the nutrients are absorbed. Here, the interface between the ambient medium and bacteria is static.

In cases where there are moving interfaces on the microscale, there are two main approaches: using a level-set formulation or explicitly tracking the position of the interface. In the level-set formulation, the moving interface is given by the zero set of a time-dependent function $f(\boldsymbol{x}, t)$, such as $f = |\boldsymbol{x}| - R(\boldsymbol{x}, t)$ in the case of an asymmetric interface with radius $R(\boldsymbol{x}, t)$, that is evolved according to the reactions that take place at the interface. In the homogenisation procedure, the key step is to utilise the separation of length scales on the microscale and the macroscale level by assuming that the variables depend on both the microscale and the macroscale independently. This assumption means that any derivative operators will then transform to a combination of derivatives with respect to the microscale and the macroscale variables. The next stage is to asymptotically expand the governing equations together with the boundary and initial conditions in powers of the ratio of the length scales, which is assumed to be a small parameter. The leading-order problem normally implies that the dependent variables are independent of the microscale variables, and thus vary only over the macroscale. A cell problem, usually involving a system of equations that arise from considering the first-order correction in the asymptotic expansion of the original system, is then formulated and needs to be solved once for a given geometry in order to extract homogenised quantities, such as effective diffusivity, that appear in the macroscale equations. The final step in the homogenisation procedure is to obtain the macroscale equations by averaging the microscale equations over the relevant microscale domain and applying the boundary conditions, which might appear at higher order in the asymptotic expansion. In the level-set formulation, the equation for the level-set function that defines the interface also needs to be expanded, and

a separate equation, which evolves the level-set function according to the reactions that take place at the interface, is necessary. The advantage of this formulation is the ability to capture spatially non-uniform evolution of any microscale interfaces. This approach has been used by van Noorden [46], for example, where he derives homogenised equations incorporating fluid flow for the evolution of a solid–liquid interface in crystal precipitation and dissolution. Similar modelling has also been done in Schultz and Knabner [44] to describe the growth, around solid particles, of a biofilm produced by mobile microorganisms that are transported in a moving fluid and can attach to, and detach from, the biofilm. They solve their cell problem, which is used to obtain effective diffusivity, until the time when the biofilms reach the boundary of the cell. In some situations, the homogenisation procedure leads to a cell problem for two variables on either side of an interface. In Bringedal *et al.* [5] and Bringedal and Kumar [6], for example, they derive and numerically solve effective macroscale equations, whose cell problem includes two domains patched together with appropriate boundary conditions.

Explicit interface tracking is often used when the evolution of the microscale interface is simple, for example, if it remains spherical. Here, the homogenisation procedure differs from the level-set formulation, because the problem can be explicitly written down in terms of the interface location, $|\boldsymbol{x}| = R(t)$, say. The interface evolution is often determined by appealing to conservation of mass and incorporating the effect of the reactions that occur on the interface. Another feature of this approach is that the unit normal to the interface needs to be expanded in both microscale and macroscale variables to take into account variations occurring over the macroscale. The rest of the homogenisation procedure follows that for the level-set formulation and consists of formulating a cell problem and averaging over the microscale domain, where the only difference is that the relevant boundary conditions can be applied at the explicit interface location. For example, in Luckins *et al.* [29], the problem of removal of toxic contaminant in a porous medium using a cleanser is considered. The removal is modelled using a first-order (linear) reaction between the two phases that occurs on the interface between them. They obtain a homogenised model that describes the effective removal of the toxic component in the case when it is surrounded by a layer of cleanser, and in the case when there is a sharp macroscale interface between the two phases. In van Noorden [47] and van Noorden [48], they obtain a one-dimensional equation for deposition and detachment in a biofilm that coats a thin pore and is subject to fluid flow.

For our filter problem, we need to solve for the sulphur dioxide concentration in both the gas and the liquid media, along with the position of the interface between them which moves due to the production of liquid sulphuric acid on the surface of the pellets that eventually become submerged by the produced liquid. This is fundamentally different to the situation studied in [29], where the reaction occurs at the interface, or [14], where it occurs in the whole bacterial region with a static interface.

In this paper, we will adopt a classical homogenisation-based approach in which we treat the filter medium as an array of cubic cells each containing a spherical pellet coated with a growing uniform layer of liquid sulphuric acid. We will exploit the separation of length scales on the pore and the device level and use homogenisation theory to derive averaged equations for the concentration of sulphur dioxide and the thickness of the acid layer within the filter. In Section 2, we will present a mathematical model for the microscale problem in the porous sheets. We will non-dimensionalise the model in Section 3 and introduce the key dimensionless parameters governing the behaviour of the system. In Section 4, we will use homogenisation to

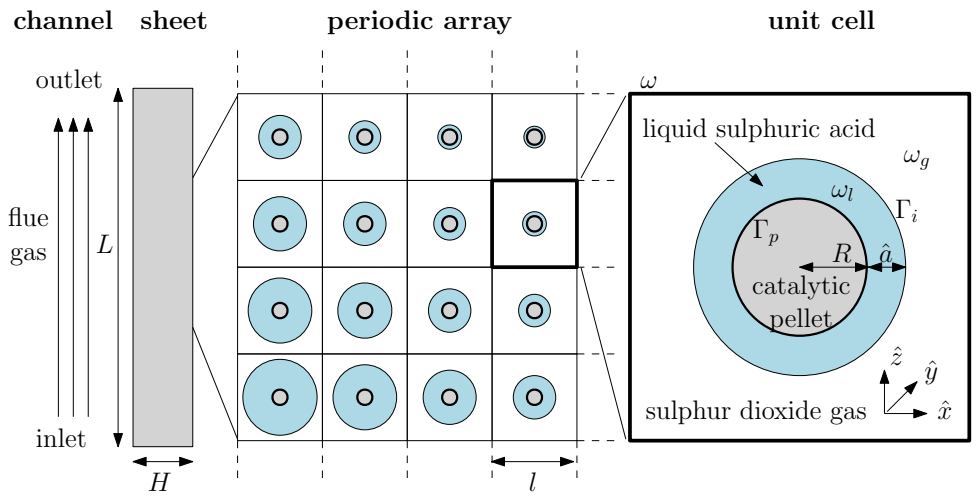

FIGURE 2. *Schematic cross-sectional representation of the porous structure of the filter. The catalytic pellets (grey) are held together by a network of fibres, not shown in the schematic.*

obtain averaged equations for the concentration of sulphur dioxide and the thickness of the liquid-acid layer throughout the filter. We will identify two distinct regimes of operation and derive the equations corresponding to each of them. In Section 5, we will couple the macroscale equations describing the filter with an equation for the gas flow in the filter channels. We will consider various model reductions, based on the filter geometry, in Section 6, and present numerical solutions and comparison with analytical results in Section 7. We will finish by discussing our results and draw conclusions in Section 8.

2. Microscale Model. Our aim is to obtain a homogenised model for the operation of the filter device (see Figure 2 left) that incorporates the effect of the porous microstructure of the filter sheets (see Figure 2 middle). We begin by presenting the mathematical model that holds in a microscopic region within the filter sheets containing a single spherical pellet (see Figure 2 right). We suppose that the microscale problem is periodic in a cubic cell of size l (taken to be the average inter-pellet distance) containing the pellet of radius $R < l/2$ at the centre, where we ignore the presence of the surrounding scaffold of thin fibres. We assume that l is much smaller than the typical thickness, width, and length of the filter sheets, H, W, and L, respectively. We represent the filter sheet as a periodic array of these cubic cells and employ a Cartesian coordinate system $(\hat{x}, \hat{y}, \hat{z})$ in each of them. We assume that the pellet catalyses the reaction presented in (1.1), and a layer of thickness $\hat{a}$ of liquid sulphuric acid forms around the pellet. We assume that surface tension tends to keep the gas–liquid interface spherical to a good approximation. We denote the cubic cell and its boundary by ω and $\partial\omega$, respectively, and the regions of gas and liquid, the interface between the two phases, and the surface of the pellet in a single cell by $\omega_g, \omega_l, \Gamma_i, \Gamma_p$, respectively, as shown in Figure 2 (right). We denote the concentration of sulphur dioxide in the gas and the liquid by $\hat{s}_g$ and $\hat{s}_l$, respectively. We assume that sulphur dioxide is transported by diffusion and advection induced by the liquid production at

the surface of the pellet. Thus, we have the following governing equations

$$\frac{\partial \hat{s}_g}{\partial \hat{t}} + \nabla \cdot (\hat{\boldsymbol{u}}_{\boldsymbol{g}} \hat{s}_g) = D_{s_g} \nabla^2 \hat{s}_g \qquad \text{in} \qquad \omega_g, \tag{2.1}$$

$$\frac{\partial \hat{s}_l}{\partial \hat{t}} + \nabla \cdot (\hat{\boldsymbol{u}}_{\boldsymbol{l}} \hat{s}_l) = D_{s_l} \nabla^2 \hat{s}_l \qquad \text{in} \qquad \omega_l, \tag{2.2}$$

where $\hat{\boldsymbol{u}}_{\boldsymbol{g}}$ and $\hat{\boldsymbol{u}}_{\boldsymbol{l}}$ are the velocities of the gas and the liquid phase, respectively, D_{s_g} and D_{s_l} are the corresponding diffusivities of sulphur dioxide in the gas and the liquid, respectively, and $\hat{t}$ denotes time. We assume that the fluid in both phases is incompressible but will not write in full the equations satisfied by $\hat{\boldsymbol{u}}_{\boldsymbol{g}}$, $\hat{\boldsymbol{u}}_{\boldsymbol{l}}$, since, as we shall see, the advection terms in (2.1) and (2.2) will be negligible in the physical limit that we consider in which the liquid layer around the catalytic pellet grows slowly. We assume that water vapour and oxygen are abundant in the system and, thus, assume that their concentrations are constant. We use the Law of Mass Action to determine the flux, $\hat{Q}$, of sulphur dioxide removed from the system at the surface of the pellets, which gives us that

$$\hat{Q} = 2k \left(\hat{s}_l|_{|\hat{\boldsymbol{x}}|=R} \right)^2, \tag{2.3}$$

where k is the reaction constant, with units $\mathrm{m}^4\,\mathrm{mol}^{-1}\,\mathrm{s}^{-1}$. We close the system using a global conservation law that links the growth of the liquid layer to the amount of liquid produced on the surface of the catalytic pellet, namely

$$\frac{\mathrm{d}}{\mathrm{d}\hat{t}} \left(\frac{4\pi\rho}{3} \left((R+\hat{a})^3 - R^3 \right) \right) = \int_{\Gamma_p} \rho V_m \hat{Q} \, \mathrm{d}\hat{S} = 4\pi\rho R^2 V_m \hat{Q}, \tag{2.4}$$

where ρ is the density of sulphuric acid, with units $\mathrm{kg\,m}^{-3}$, and V_m is the molar volume of liquid sulphuric acid, with units $\mathrm{m}^3\,\mathrm{mol}^{-1}$. We note that we can ignore the mass of the dissolved sulphur dioxide in this calculation, because, in one cubic metre of liquid sulphuric acid, there are approximately 16g of sulphur dioxide, compared to the 1830kg of acid [34]. We rewrite (2.4) as

$$\frac{\mathrm{d}\hat{a}}{\mathrm{d}\hat{t}} = \frac{2V_m k \left(\hat{s}_l|_{|\hat{\boldsymbol{x}}|=R} \right)^2}{(1+\hat{a}/R)^2}. \tag{2.5}$$

At the pellet's surface, the velocity of the liquid is given by its production rate

$$\hat{\boldsymbol{u}}_{\boldsymbol{l}} \cdot \boldsymbol{n}_p = 2V_m k \hat{s}_l^2, \tag{2.6}$$

where $\boldsymbol{n}_p$ denotes the outwards-pointing unit vector to the surface of the pellet, which is in the radial direction $\boldsymbol{e}_r$. At the surface of the pellet, we balance the flux of sulphur dioxide into the pellet with the amount being consumed by the reaction, i.e.,

$$(D_{s_l} \nabla \hat{s}_l - \hat{\boldsymbol{u}}_{\boldsymbol{l}} \hat{s}_l) \cdot \boldsymbol{n}_p = 2k \hat{s}_l^2, \tag{2.7}$$

which we can rewrite, using (2.6), to be

$$D_{s_l} \nabla \hat{s}_l \cdot \boldsymbol{n}_p = 2k(1 + V_m s_l) \hat{s}_l^2. \tag{2.8}$$

At the gas–liquid interface, we impose continuity of flux of sulphur dioxide, and we assume local thermodynamic equilibrium (which leads to Henry's law) and, thus,

we write

$$-D_{s_g}\nabla\hat{s}_g\cdot\boldsymbol{n}_i=-D_{s_l}\nabla\hat{s}_l\cdot\boldsymbol{n}_i, \tag{2.9}$$

$$\hat{s}_g=\beta_s\hat{s}_l, \tag{2.10}$$

where β_s is a partition coefficient, which measures the relative solubility of the gas in each phase, and

$$\boldsymbol{n}_i=\frac{\nabla\left(|\hat{\boldsymbol{x}}|-R-\hat{a}\right)}{|\nabla\left(|\hat{\boldsymbol{x}}|-R-\hat{a}\right)|} \tag{2.11}$$

denotes the outwards-pointing unit normal to the liquid layer.

To close the microscale model, we prescribe periodicity of $\hat{s}_g$ along the boundary of each cell and also assume

$$\hat{s}_g=S_0\quad\text{and}\quad\hat{a}=0\qquad\text{at}\qquad\hat{t}=0, \tag{2.12}$$

where S_0 is the inlet concentration of sulphur dioxide. Once we obtain the macroscale equations that hold over the domain of the whole device in Section 5, we will prescribe the necessary macroscale boundary and initial conditions.

We present typical values of the physical parameters in Table 1. We note that the sulphur dioxide concentration may be smaller than the quoted value by one or two orders of magnitude depending on the level of contamination, and the inter-pellet distance can be smaller by an order of magnitude, so that it is comparable to the radius of the pellets.

Parameter	Definition	Value	Units
β_s	Henry's law constant for sulphur dioxide	4×10^{-2}	–
D_{s_g}	Diffusivity of sulphur dioxide in air	1×10^{-5}	$\mathrm{m^2\,s^{-1}}$
D_{s_l}	Diffusivity of sulphur dioxide in liquid sulphuric acid	2×10^{-9}	$\mathrm{m^2\,s^{-1}}$
V_m	Molar volume of sulphuric acid	5×10^{-5}	$\mathrm{m^3\,mol^{-1}}$
d	Radius of filter channels	5×10^{-3}	m
k	Rate of chemical reaction	5×10^{-5}	$\mathrm{m^4\,mol^{-1}\,s^{-1}}$
l	Inter-pellet distance	5×10^{-5}	m
H	Thickness of filter sheet	10^{-3}	m
L	Length of filter channels	3×10^{-1}	m
R	Pellets radius	5×10^{-6}	m
S_0	Inlet concentration of sulphur dioxide in the filter channels	10^{-2}	$\mathrm{mol\,m^{-3}}$
U	Speed of gas flow in filter channels	3×10^{-1}	$\mathrm{m\,s^{-1}}$
W	Width of filter sheet	1×10^{-2}	m

TABLE 1

Parameter values (taken from [28, 30, 34, 42]). Note that k is an effective rate, and its value is determined indirectly from experimental data.

3. Dimensionless Model. We non-dimensionalise (2.1), (2.2), (2.5)–(2.10), and (2.12) using

$$(\hat{\boldsymbol{x}},\hat{a})=l\,(\boldsymbol{x},a)\,,\quad \hat{t}=\left(\beta_s^2 l/V_m k S_0^2\right)t,\quad \hat{s}_g=S_0 s_g,\quad \hat{s}_l=\left(S_0/\beta_s\right)s_l,\quad (\hat{\boldsymbol{u}}_{\boldsymbol{g}},\hat{\boldsymbol{u}}_{\boldsymbol{l}})=\left(V_m k S_0^2/\beta_s^2\right)(\boldsymbol{u}_{\boldsymbol{g}},\boldsymbol{u}_{\boldsymbol{l}}), \tag{3.1}$$

where we have chosen to nondimensionalise using the timescale over which the liquid layer grows to fill the void space. Using the typical parameter values in Table 1 we find this timescale is approximately equal to 3.7 days, which is longer than the timescale for diffusive gas transport ($l^2/D_{s_g} = 2.5 \times 10^{-4}$s). The dimensionless model reads

$$\nu^2\eta\left(\frac{\partial s_g}{\partial t} + \boldsymbol{u_g}\cdot\nabla s_g\right) = \nabla^2 s_g \qquad \text{in} \qquad \omega_g, \tag{3.2}$$

$$\nu^2\left(\frac{\partial s_l}{\partial t} + \boldsymbol{u_l}\cdot\nabla s_l\right) = \nabla^2 s_l \qquad \text{in} \qquad \omega_l, \tag{3.3}$$

$$\frac{\mathrm{d}a}{\mathrm{d}t} = \frac{2\left(s_l|_{|\boldsymbol{x}|=\lambda}\right)^2}{(1+a/\lambda)^2}, \tag{3.4}$$

subject to the boundary conditions and initial conditions

$$\nabla s_l\cdot\boldsymbol{n}_p = 2\left(\kappa_s + \nu^2 s_l\right)s_l^2 \qquad \text{on} \qquad \Gamma_p, \tag{3.5}$$

$$-\nabla s_g\cdot\boldsymbol{n}_i = -\frac{\eta}{\beta_s}\nabla s_l\cdot\boldsymbol{n}_i \qquad \text{on} \qquad \Gamma_i, \tag{3.6}$$

$$s_g = s_l \qquad \text{on} \qquad \Gamma_i, \tag{3.7}$$

$$s_g \text{ periodic} \qquad \text{on} \qquad \partial\omega, \tag{3.8}$$

$$s_g = 1 \qquad \text{at} \qquad t = 0, \tag{3.9}$$

$$a = 0 \qquad \text{at} \qquad t = 0, \tag{3.10}$$

where we have introduced the following four dimensionless parameters:

$$\eta = \frac{D_{s_l}}{D_{s_g}} \approx 10^{-4}, \quad \kappa_s = \frac{klS_0}{\beta_s D_{s_l}} \approx 10^{-1}, \quad \lambda = \frac{R}{l} \approx 10^{-1}, \quad \nu = \sqrt{\frac{V_m klS_0^2}{\beta_s^2 D_{s_l}}} \approx 10^{-2}. \tag{3.11}$$

Here, η is the ratio of the diffusivities of sulphur dioxide in the liquid and gas phase, κ_s (sometimes called a Damköhler number) measures the relative strength of the reaction on the surface of the pellet to diffusion of sulphur dioxide in the liquid sulphuric acid, λ is a measure of how densely packed the catalytic pellets are, and ν is the Péclet number,[1] i.e., the ratio of the diffusive timescale in the liquid over the pore scale to the timescale associated with the liquid-layer growth. We also introduce the ratio of the pore length scale to the filter sheet thickness, $\epsilon = l/H \approx 5\times10^{-2} \ll 1$, which we will use later in the homogenisation. We note that $\nu = \epsilon\sqrt{\tau}$, where $\tau = V_m kH^2 S_0^2/\beta_s^2 l D_{s_l}$ is the ratio of the diffusive timescale in the liquid over the thickness of the filter sheet to the timescale associated with the liquid-layer growth.

4. Homogenisation. Our goal is to obtain macroscale equations, valid over the whole filter domain, by averaging over the complicated porous microstructure of the filter sheets, in order to obtain the effective removal of sulphur dioxide by the filter. We introduce the macroscale spatial variables

$$\boldsymbol{X} = \epsilon\boldsymbol{x}, \tag{4.1}$$

and let s_g, s_l, and a also depend independently on the macroscale variables. Using (4.1) together with the Chain Rule, the gradient operator transforms as $\nabla \to \nabla_x +$

[1] We have used ν here for the Péclet number, reserving Pe for the Péclet number in the outer flow, as described in Section 5.

$\epsilon\nabla_X$. We also note that, using the fact that $\nabla_x|\boldsymbol{x}| = \boldsymbol{x}/|\boldsymbol{x}| = \boldsymbol{e}_r$,

$$\nabla\left(|\boldsymbol{x}| - \lambda - a\right) = \boldsymbol{e}_r - \epsilon\nabla_X a, \tag{4.2}$$

and we see that, due to the dependence on the macroscale variables, $\boldsymbol{n}_i$, defined by (2.11) is not equal to $\boldsymbol{e}_r$. Rewriting (3.2)–(3.8), we have

$$\begin{aligned}
&\epsilon^2\tau\eta\left(\frac{\partial s_g}{\partial t} + \boldsymbol{u_g}\cdot\left(\nabla_x + \epsilon\nabla_X\right)s_g\right)\\
&\quad = \nabla_x^2 s_g + \epsilon\left(\nabla_x\cdot\nabla_X + \nabla_X\cdot\nabla_x\right)s_g + \epsilon^2\nabla_X^2 s_g \qquad \text{in} \qquad \omega_g, \qquad (4.3)\\
&\epsilon^2\tau\left(\frac{\partial s_l}{\partial t} + \boldsymbol{u_l}\cdot\left(\nabla_x + \epsilon\nabla_X\right)s_l\right)\\
&\quad = \nabla_x^2 s_l + \epsilon\left(\nabla_x\cdot\nabla_X + \nabla_X\cdot\nabla_x\right)s_l + \epsilon^2\nabla_X^2 s_l \qquad \text{in} \qquad \omega_l, \qquad (4.4)
\end{aligned}$$

$$\frac{\partial a}{\partial t} = \frac{2\left(s_l|_{|\boldsymbol{x}|=\lambda}\right)^2}{(1+a/\lambda)^2}, \tag{4.5}$$

subject to the boundary conditions

$$\left(\nabla_x + \epsilon\nabla_X\right)s_l\cdot\boldsymbol{e}_r = 2\left(\kappa_s + \epsilon^2\tau s_l\right)s_l^2 \quad \text{on} \quad \Gamma_p, \tag{4.6}$$

$$-\left(\nabla_x + \epsilon\nabla_X\right)s_g\cdot\left(\boldsymbol{e}_r - \epsilon\nabla_X a\right) = -\frac{\eta}{\beta_s}\left(\nabla_x + \epsilon\nabla_X\right)s_l\cdot\left(\boldsymbol{e}_r - \epsilon\nabla_X a\right) \quad \text{on} \quad \Gamma_i, \tag{4.7}$$

$$s_g = s_l \quad \text{on} \quad \Gamma_i, \tag{4.8}$$

$$s_g \text{ is periodic} \quad \text{on} \quad \partial\omega, \tag{4.9}$$

and the initial conditions (3.9) and (3.10), which we will not explicitly mention again until we derive the macroscale equations.

For the richest asymptotic limit, we begin by assuming that $\tau = O(1)$ and $\eta = O(1)$. The case when these parameters are small, which is the case for the physical experiments (see (3.11)), corresponds to a sub-limit that can easily be obtained from our more general results. At the end of the section, we will also mention another physically less relevant limit when $\tau \gg 1$ and $\eta \ll 1$. However, in this case little analytical progress can be made due to the non-linearity in the system of equations and boundary conditions. The parameters that most significantly control the behaviour of our system are η/β_s and κ_s, as they dictate respectively how much and how fast sulphur dioxide can be transported to the pellets in order to produce liquid sulphuric acid that eventually clogs up the filter. There is a rich underlying asymptotic structure associated with the order of magnitude of these parameters. In particular, we will find later on that, if the product of these parameters, $\sigma_s\kappa_s$ (where $\sigma_s = \eta/\beta_s$) is not sufficiently small, then sulphur dioxide is completely consumed in the filter medium, and non-zero solutions appear as higher-order corrections only. This, for example, corresponds to the case when the dimensionless rate of mass transfer of sulphur dioxide into the liquid is $O(1)$ and comparable to the rate at which it is being consumed by the reaction. It transpires that, when $\sigma_s\kappa_s = O(\epsilon^2)$, we have a non-trivial behaviour at leading order in the sulphur dioxide concentration in both the gas and the liquid phases. We, therefore, first present two distinguished limits when $\sigma_s\kappa_s = O(\epsilon^2)$, and then briefly discuss what happens when $\sigma_s\kappa_s \gg \epsilon^2$.

4.1. Limit I: $\boldsymbol{\sigma_s = O(\epsilon^2)}$ and $\boldsymbol{\kappa_s = O(1)}$. We begin by exploring the case when the mass transfer of sulphur dioxide into the liquid $\sigma_s = O(\epsilon^2)$, but the dimensionless reaction rate $\kappa_s = O(1)$. For convenience, we write $\sigma_s = \epsilon^2\tilde{\sigma}_s$, where

$\tilde{\sigma}_s = O(1)$. We expand each of the dependent variables in (4.3)–(4.9) as

$$f \sim f^{(0)} + \epsilon f^{(1)} + \epsilon^2 f^{(2)} + \cdots, \tag{4.10}$$

and obtain the following leading-order problem for s_g, s_l, and a:

$$\nabla_x^2 s_g^{(0)} = 0 \qquad \text{in} \qquad \omega_g^{(0)}, \tag{4.11}$$

$$\nabla_x^2 s_l^{(0)} = 0 \qquad \text{in} \qquad \omega_l^{(0)}, \tag{4.12}$$

$$\frac{\partial a^{(0)}}{\partial t} = \frac{2\left(s_l^{(0)}|_{|\boldsymbol{x}|=\lambda}\right)^2}{(1+a^{(0)}/\lambda)^2}, \tag{4.13}$$

subject to the boundary conditions

$$\nabla_x s_l^{(0)} \cdot \boldsymbol{e}_r = 2\kappa_s s_l^{(0)2} \qquad \text{on} \qquad \Gamma_p, \tag{4.14}$$

$$-\nabla_x s_g^{(0)} \cdot \boldsymbol{e}_r = 0 \qquad \text{on} \qquad \Gamma_i^{(0)}, \tag{4.15}$$

$$s_g^{(0)} = s_l^{(0)} \qquad \text{on} \qquad \Gamma_i^{(0)}, \tag{4.16}$$

$$s_g^{(0)} \text{ is periodic} \qquad \text{on} \qquad \partial\omega, \tag{4.17}$$

where $\omega_g^{(0)} = \omega \backslash \{|\boldsymbol{x}| \leq \lambda + a^{(0)}\}$, $\omega_l^{(0)} = \{\lambda < |\boldsymbol{x}| < \lambda + a^{(0)}\}$, and $\Gamma_i^{(0)} = \{|\boldsymbol{x}| = \lambda + a^{(0)}\}$. We first solve the problem in the liquid layer. We rewrite (4.12) in spherical polar coordinates, assume radial symmetry, integrate, and apply (4.14) to find that

$$\frac{\partial s_l^{(0)}}{\partial r} = \frac{2\lambda^2\kappa_s\left(s_l^{(0)}|_{r=\lambda}\right)^2}{r^2}, \tag{4.18}$$

where we note that, due to radial symmetry, $s_l^{(0)}|_{r=\lambda}$ is a function of the macroscale variables only.

Integrating once again and using (4.16), we obtain

$$s_l^{(0)} = 2\lambda^2\kappa_s\left(s_l^{(0)}|_{r=\lambda}\right)^2\left(\frac{1}{\lambda + a^{(0)}} - \frac{1}{r}\right) + s_g^{(0)}|_{r=\lambda+a^{(0)}}. \tag{4.19}$$

Evaluating (4.19) at $r = \lambda$ yields a quadratic equation for $s_l^{(0)}|_{r=\lambda}$ that has one physically relevant solution, which is non-negative and bounded as $\kappa_s \to 0$. Rewriting (4.19), evaluated at $r = \lambda$, in the form

$$s_l^{(0)}|_{r=\lambda} = \left(\frac{\lambda + a^{(0)}}{2a^{(0)}\lambda\kappa_s}\right)^{1/2}\left(s_g^{(0)}|_{r=\lambda+a^{(0)}} - s_l^{(0)}|_{r=\lambda}\right)^{1/2}, \tag{4.20}$$

and substituting the solution to (4.19) in the right-hand side of (4.20) yields

$$s_l^{(0)}|_{r=\lambda} = \frac{1+a^{(0)}/\lambda}{2\sqrt{2}\kappa_s a^{(0)}}\left(1 + \frac{4\lambda\kappa_s a^{(0)} s_g^{(0)}|_{r=\lambda+a^{(0)}}}{\lambda + a^{(0)}} - \sqrt{1 + \frac{8\lambda\kappa_s a^{(0)} s_g^{(0)}|_{r=\lambda+a^{(0)}}}{\lambda + a^{(0)}}}\right)^{\frac{1}{2}}. \tag{4.21}$$

Now considering (4.11), we multiply both sides by $s_g^{(0)}$, integrate over $\omega_g^{(0)}$, use the Divergence Theorem and rearrange to obtain

$$\iiint_{\omega_g^{(0)}} \left|\nabla_x s_g^{(0)}\right|^2 \mathrm{d}V = \iint_{\partial\omega_g^{(0)}} s_g^{(0)} \nabla_x s_g^{(0)} \cdot \mathbf{d}\boldsymbol{S}. \tag{4.22}$$

Since $s_g^{(0)}$ is periodic on the boundary of the unit cell ω, the surface integral in (4.22) over $\partial\omega$ evaluates to zero. On $\Gamma_i^{(0)} = \{|\boldsymbol{x}| = \lambda + a^{(0)}\}$, we use (4.15) to obtain

$$\iiint_{\omega_g^{(0)}} \left|\nabla_x s_g^{(0)}\right|^2 \,\mathrm{d}V = 0. \tag{4.23}$$

Thus,

$$s_g^{(0)} = s_g^{(0)}(\boldsymbol{X}, t), \tag{4.24}$$

i.e., $s_g^{(0)}$ depends only on the macroscale spatial variables. We manipulate (4.21) (utilising the formula $A - B = \left(A^2 - B^2\right)/\left(A + B\right)$) to find

$$s_l^{(0)}|_{r=\lambda} = \sqrt{2} s_g^{(0)} \left(1 + \frac{4\lambda\kappa_s a^{(0)} s_g^{(0)}}{\lambda + a^{(0)}} + \sqrt{1 + \frac{8\lambda\kappa_s a^{(0)} s_g^{(0)}}{\lambda + a^{(0)}}}\right)^{-\frac{1}{2}}, \tag{4.25}$$

where we have rationalised $s_l^{(0)}|_{r=\lambda}$ to further simplify it.

We now consider the $O(\epsilon)$ terms in (4.3)–(4.9) in order to determine the problem for $s_g^{(1)}$. We have

$$\nabla_x^2 s_g^{(1)} = 0 \qquad \text{in} \qquad \omega_g^{(0)}, \tag{4.26}$$

subject to the boundary conditions

$$-\left(\nabla_X s_g^{(0)} + \nabla_x s_g^{(1)}\right) \cdot \boldsymbol{e}_r = 0 \qquad \text{on} \qquad \Gamma_i^{(0)}, \tag{4.27}$$

$$s_g^{(1)} \text{ is periodic} \qquad \text{on} \qquad \partial\omega. \tag{4.28}$$

We use the linearity of the problem for $s_g^{(1)}$ to write the solution in the form

$$s_g^{(1)} = \boldsymbol{\Phi} \cdot \nabla_X s_g^{(0)}, \tag{4.29}$$

where the function $\boldsymbol{\Phi}(\boldsymbol{x}, t) = (\Phi_1, \Phi_2, \Phi_3)$ satisfies the cell problem

$$\nabla_x^2 \Phi_i = 0 \qquad \text{in} \qquad \omega_g^{(0)}, \tag{4.30}$$

subject to

$$\left(\nabla_x \Phi_i + \boldsymbol{e}_i\right) \cdot \boldsymbol{e}_r = 0 \qquad \text{on} \qquad \Gamma_i^{(0)}, \tag{4.31}$$

$$\Phi_i \text{ is periodic} \qquad \text{on} \qquad \partial\omega, \tag{4.32}$$

for $i = 1, 2, 3$, and where $\boldsymbol{e}_i$ is the unit vector in the x, y, z direction, respectively.

We now look at the $O(\epsilon^2)$ terms in (4.3)–(4.9) in order to determine the problem for $s_g^{(2)}$. We have

$$\tau\eta \frac{\partial s_g^{(0)}}{\partial t} = \nabla_x^2 s_g^{(2)} + \left(\nabla_x \cdot \nabla_X + \nabla_X \cdot \nabla_x\right) s_g^{(1)} + \nabla_X^2 s_g^{(0)} \qquad \text{in} \qquad \omega_g^{(0)}, \tag{4.33}$$

subject to the boundary conditions

$$\begin{aligned} &-\left(\nabla_x s_g^{(2)} + \nabla_X s_g^{(1)}\right) \cdot \boldsymbol{e}_r + \nabla_X a^{(0)} \cdot \left(\nabla_x s_g^{(1)} + \nabla_X s_g^{(0)}\right) \\ &\qquad = -\tilde{\sigma}_s \nabla_x s_l^{(0)} \cdot \boldsymbol{e}_r = -\frac{2\tilde{\sigma}_s \kappa_s \left(s_l^{(0)}|_{r=\lambda}\right)^2}{\left(1 + a^{(0)}/\lambda\right)^2} \qquad \text{on} \qquad \Gamma_i^{(0)}, \end{aligned} \tag{4.34}$$

$$s_g^{(2)} \text{ is periodic} \qquad \text{on} \qquad \partial\omega, \tag{4.35}$$

where we have used (4.18) and (4.27) to simplify (4.34) and remove the terms that come from expanding s_g on the boundary $\Gamma_i^{(0)} = \{|\boldsymbol{x}| = \lambda + a^{(0)}\}$.

We now integrate (4.33) over $\omega_g^{(0)}$, remembering that $s_g^{(0)}$ does not depend on the microscale variables, and use the Divergence Theorem to obtain

$$\tau\eta\mathcal{V}_g\frac{\partial s_g^{(0)}}{\partial t} = \iiint_{\omega_g^{(0)}} \nabla_X \cdot \left(\nabla_x s_g^{(1)} + \nabla_X s_g^{(0)}\right) \mathrm{d}V + \iint_{\partial\omega_g^{(0)}} \left(\nabla_X s_g^{(1)} + \nabla_x s_g^{(2)}\right) \cdot \mathbf{d}\boldsymbol{S}, \tag{4.36}$$

where

$$\mathcal{V}_g\left(\omega_g^{(0)}\right) = \iiint_{\omega_g^{(0)}} \mathrm{d}V \tag{4.37}$$

is the volume of the gas phase in the unit cell. To rewrite the volume integral in (4.36), we use a generalisation of Leibniz' Rule in the form

$$\nabla_X \cdot \iiint_{\omega_g^{(0)}(\boldsymbol{X},t)} \boldsymbol{g}\left(\boldsymbol{X},\boldsymbol{x},t\right) \mathrm{d}V = \iiint_{\omega_g^{(0)}} \nabla_X \cdot \boldsymbol{g}\, \mathrm{d}V - \iint_{\{|\boldsymbol{x}|=\lambda+a^{(0)}\}} \nabla_X a^{(0)} \cdot \boldsymbol{g}\, \mathrm{d}S. \tag{4.38}$$

With $\boldsymbol{g} = \nabla_x s_g^{(1)} + \nabla_X s_g^{(0)}$, we obtain

$$\begin{aligned}
\iiint_{\omega_g^{(0)}} \nabla_X \cdot \left(\nabla_x s_g^{(1)} + \nabla_X s_g^{(0)}\right) \mathrm{d}V &= \nabla_X \cdot \iiint_{\omega_g^{(0)}} \nabla_x s_g^{(1)} + \nabla_X s_g^{(0)}\, \mathrm{d}V \\
&\quad + \iint_{\Gamma_i^{(0)}} \nabla_X a^{(0)} \cdot \left(\nabla_x s_g^{(1)} + \nabla_X s_g^{(0)}\right) \mathrm{d}S \\
&= \nabla_X \cdot \left(\mathcal{V}_g \left(\mathbf{I} + \frac{1}{\mathcal{V}_g} \iiint_{\omega_g^{(0)}} \nabla_x \boldsymbol{\Phi}\, \mathrm{d}V\right) \nabla_X s_g^{(0)}\right) \\
&\quad + \iint_{\Gamma_i^{(0)}} \nabla_X a^{(0)} \cdot \left(\nabla_x s_g^{(1)} + \nabla_X s_g^{(0)}\right) \mathrm{d}S,
\end{aligned} \tag{4.39}$$

where $\mathbf{I}$ is the identity matrix, and we have used (4.29) to obtain the final line in (4.39). Since $s_g^{(1)}$ and $s_g^{(2)}$ are periodic on $\partial\omega$, the surface integral in (4.36) can be reduced to an integral over $\Gamma_i^{(0)}$ only and so, using (4.34), we find that

$$\begin{aligned}
\iint_{\partial\omega_g^{(0)}} \left(\nabla_X s_g^{(1)} + \nabla_x s_g^{(2)}\right) \cdot \mathbf{d}\boldsymbol{S} &= -\frac{2\tilde{\sigma}_s\kappa_s \left(s_l^{(0)}|_{r=\lambda}\right)^2 \mathcal{S}_{gl}}{\left(1 + a^{(0)}/\lambda\right)^2} \\
&\quad - \iint_{\Gamma_i^{(0)}} \nabla_X a^{(0)} \cdot \left(\nabla_x s_g^{(1)} + \nabla_X s_g^{(0)}\right) \mathrm{d}S,
\end{aligned} \tag{4.40}$$

where

$$\mathcal{S}_{gl}\left(\Gamma_i^{(0)}\right) = \iint_{\Gamma_i^{(0)}} \mathrm{d}S \tag{4.41}$$

is the surface area of the gas–liquid interface. Rewriting (4.36), using (4.39) and (4.40), we obtain the macroscale equations that govern the evolution of $s_g^{(0)}$ and $a^{(0)}$,

which, dropping the superscripts, read

$$\tau\eta\frac{\partial s_g}{\partial t} = \frac{1}{\mathcal{V}_g}\nabla_X\cdot\left(\mathcal{V}_g\mathbf{D}\nabla_X s_g\right) - \frac{2\tilde{\sigma}_s\kappa_s\left(s_l|_{r=\lambda}\right)^2\mathcal{S}_{gl}}{\mathcal{V}_g\left(1+a/\lambda\right)^2}, \tag{4.42}$$

$$\frac{\partial a}{\partial t} = \frac{2\left(s_l|_{r=\lambda}\right)^2}{(1+a/\lambda)^2}, \tag{4.43}$$

where

$$\mathbf{D}_{ij} = \delta_{ij} + \frac{1}{\mathcal{V}_g}\iiint_{\omega_g}\frac{\partial\Phi_j}{\partial x_i}\,\mathrm{d}V, \tag{4.44}$$

is the macroscopic diffusivity tensor which depends on the microscale structure, δ_{ij} is the Kronecker delta,

$$\mathcal{V}_g = 1 - \frac{4}{3}\pi\left(\lambda+a\right)^3, \qquad \mathcal{S}_{gl} = 4\pi\left(\lambda+a\right)^2, \tag{4.45}$$

and $s_l|_{r=\lambda}$ is given by (4.25). Due to the spatial symmetry of the cubic cell, $\mathbf{D}$ is proportional to the identity matrix, i.e., $\mathbf{D} = D\mathbf{I}$. We solve for D numerically using COMSOL Multiphysics. In Figure 3, we plot D as a function of $\lambda+a$, and we observe that D decreases as the liquid layer increases in thickness, as expected.

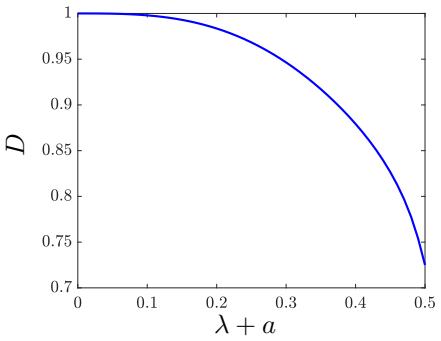

FIGURE 3. *Effective diffusivity, D, as a function of the dimensionless radius of the pellet and thickness of the liquid layer around it.*

We conclude with a remark about the physical significance of the variable s_g. Since s_g is independent of the microscale, it can be related to the volume average of the sulphur dioxide concentration over the gas phase (which is an experimentally measurable quantity), by

$$s_g = \frac{1}{\mathcal{V}_g}\iiint_{\omega_g} s_g\,\mathrm{d}V. \tag{4.46}$$

Another useful quantity is the volume-averaged concentration over the whole space, defined as

$$S_g = \frac{1}{\mathcal{V}}\left(\iiint_{\omega_g} s_g\,\mathrm{d}V + \iiint_{\omega_l} s_l\,\mathrm{d}V\right) = \mathcal{V}_g s_g + \iiint_{\omega_l} s_l\,\mathrm{d}V, \tag{4.47}$$

since $\mathcal{V}=1$ is the volume of ω. S_g is important when we are interested in the total amount of sulphur dioxide in the filter, in both gaseous and dissolved form.

4.2. Limit II: $\sigma_s = O(1)$ and $\kappa_s = O(\epsilon^2)$. The second distinguished limit is the case when the mass transfer of sulphur dioxide into the liquid happens at an $O(1)$ rate and the dimensionless reaction rate is small. For convenience, we write $\kappa_s = \epsilon^2 \tilde{\kappa}_s$, where $\tilde{\kappa}_s = O(1)$. In this case, the $O(1)$ problem for s_g, s_l, and a becomes

$$\nabla_x^2 s_g^{(0)} = 0 \qquad \text{in} \qquad \omega_g^{(0)}, \tag{4.48}$$

$$\nabla_x^2 s_l^{(0)} = 0 \qquad \text{in} \qquad \omega_l^{(0)}, \tag{4.49}$$

$$\frac{\partial a^{(0)}}{\partial t} = \frac{2\left(s_l^{(0)}|_{r=\lambda}\right)^2}{(1+a^{(0)}/\lambda)^2}, \tag{4.50}$$

subject to the boundary conditions

$$\nabla_x s_l^{(0)} \cdot \boldsymbol{e}_r = 0 \qquad \text{on} \qquad \Gamma_p, \tag{4.51}$$

$$-\nabla_x s_g^{(0)} \cdot \boldsymbol{e}_r = -\sigma_s \nabla_x s_l^{(0)} \cdot \boldsymbol{e}_r \qquad \text{on} \qquad \Gamma_i^{(0)}, \tag{4.52}$$

$$s_g^{(0)} = s_l^{(0)} \qquad \text{on} \qquad \Gamma_i^{(0)}, \tag{4.53}$$

$$s_g^{(0)} \text{ is periodic} \qquad \text{on} \qquad \partial\omega. \tag{4.54}$$

Returning to (4.48) and using (4.52) in an identical way as in Subsection 4.1, we obtain

$$\begin{aligned} \iiint_{\omega_g^{(0)}} \left|\nabla_x s_g^{(0)}\right|^2 \mathrm{d}V &= -\iint_{\Gamma_i^{(0)}} s_g^{(0)} \nabla_x s_g^{(0)} \cdot \boldsymbol{e}_r \mathrm{d}S = -\iint_{\Gamma_i^{(0)}} \sigma_s s_l^{(0)} \nabla_x s_l^{(0)} \cdot \boldsymbol{e}_r \mathrm{d}S \\ &= -\iint_{\Gamma_p} \sigma_s s_l^{(0)} \nabla_x s_l^{(0)} \cdot \boldsymbol{e}_r \mathrm{d}S = 0, \end{aligned} \tag{4.55}$$

where we have used the Divergence Theorem twice, together with (4.51) and (4.53). We conclude that $s_g^{(0)}$ is a function of the macroscale variables only. Solving the problem in the liquid layer given by (4.49), together with (4.51) and (4.53), we obtain

$$s_l^{(0)} = s_g^{(0)}. \tag{4.56}$$

We now consider the $O(\epsilon)$ problem of (4.3)–(4.9) for $s_g^{(1)}$ and $s_l^{(1)}$, namely

$$\nabla_x^2 s_g^{(1)} = 0 \qquad \text{in} \qquad \omega_g^{(0)}, \tag{4.57}$$

$$\nabla_x^2 s_l^{(1)} = 0 \qquad \text{in} \qquad \omega_l^{(0)}, \tag{4.58}$$

subject to the boundary conditions

$$(\nabla_x s_l^{(1)} + \nabla_X s_l^{(0)}) \cdot \boldsymbol{e}_r = 0 \qquad \text{on} \qquad \Gamma_p, \tag{4.59}$$

$$-\left(\nabla_X s_g^{(0)} + \nabla_x s_g^{(1)}\right) \cdot \boldsymbol{e}_r = -\sigma_s \left(\nabla_X s_l^{(0)} + \nabla_x s_l^{(1)}\right) \cdot \boldsymbol{e}_r \qquad \text{on} \qquad \Gamma_i^{(0)}, \tag{4.60}$$

$$s_g^{(1)} = s_l^{(1)} \qquad \text{on} \qquad \Gamma_i^{(0)}, \tag{4.61}$$

$$s_g^{(1)} \text{ is periodic} \qquad \text{on} \qquad \partial\omega, \tag{4.62}$$

again evaluating to zero the terms involving $\nabla_x s_l^{(0)}$ on the right-hand sides of (4.60) and (4.61) that arise from expanding the variables around the moving boundary.

In this limit, we use the linearity of the problem for both $s_g^{(1)}$ and $s_l^{(1)}$ to write the solution in the form

$$s_g^{(1)} = \boldsymbol{\Omega} \cdot \nabla_X s_g^{(0)}, \tag{4.63}$$

$$s_l^{(1)} = \boldsymbol{\Theta} \cdot \nabla_X s_l^{(0)}, \tag{4.64}$$

where the functions $\boldsymbol{\Omega}(\boldsymbol{x}, t) = (\Omega_1, \Omega_2, \Omega_3)$ and $\boldsymbol{\Theta}(\boldsymbol{x}, t) = (\Theta_1, \Theta_2, \Theta_3)$ satisfy the cell problems

$$\nabla_x^2 \Omega_i = 0 \qquad \text{in} \qquad \omega_g^{(0)}, \tag{4.65}$$

$$\nabla_x^2 \Theta_i = 0 \qquad \text{in} \qquad \omega_l^{(0)}, \tag{4.66}$$

subject to, for $i = 1, 2, 3$,

$$(\nabla_x \Omega_i + \boldsymbol{e}_i) \cdot \boldsymbol{e}_r = \sigma_s \left(\nabla_x \Theta_i + \boldsymbol{e}_i\right) \cdot \boldsymbol{e}_r \qquad \text{on} \qquad \Gamma_i^{(0)}, \tag{4.67}$$

$$\Omega_i = \Theta_i \qquad \text{on} \qquad \Gamma_i^{(0)}, \tag{4.68}$$

$$(\nabla_x \Theta_i + \boldsymbol{e}_i) \cdot \boldsymbol{e}_r = 0 \qquad \text{on} \qquad \Gamma_p, \tag{4.69}$$

$$\Omega_i \text{ is periodic} \qquad \text{on} \qquad \partial\omega. \tag{4.70}$$

We now look at the $O(\epsilon^2)$ problem of (4.3)–(4.9) for $s_g^{(2)}$ and $s_l^{(2)}$, which becomes

$$\tau\eta \frac{\partial s_g^{(0)}}{\partial t} = \nabla_x^2 s_g^{(2)} + \left(\nabla_x \cdot \nabla_X + \nabla_X \cdot \nabla_x\right) s_g^{(1)} + \nabla_X^2 s_g^{(0)} \qquad \text{in} \qquad \omega_g^{(0)}, \tag{4.71}$$

$$\tau \frac{\partial s_l^{(0)}}{\partial t} = \nabla_x^2 s_l^{(2)} + \left(\nabla_x \cdot \nabla_X + \nabla_X \cdot \nabla_x\right) s_l^{(1)} + \nabla_X^2 s_l^{(0)} \qquad \text{in} \qquad \omega_l^{(0)}, \tag{4.72}$$

subject to the relevant boundary conditions

$$\begin{aligned} &- \left(\nabla_x s_g^{(2)} + \nabla_X s_g^{(1)}\right) \cdot \boldsymbol{e}_r + \nabla_X a^{(0)} \cdot \left(\nabla_x s_g^{(1)} + \nabla_X s_g^{(0)}\right) \\ &= \sigma_s \left(- \left(\nabla_x s_l^{(2)} + \nabla_X s_l^{(1)}\right) \cdot \boldsymbol{e}_r + \nabla_X a^{(0)} \cdot \left(\nabla_x s_l^{(1)} + \nabla_X s_l^{(0)}\right)\right) \quad \text{on} \quad \Gamma_i^{(0)}, \end{aligned} \tag{4.73}$$

$$\left(\nabla_x s_l^{(2)} + \nabla_X s_l^{(1)}\right) \cdot \boldsymbol{e}_r = 2\left(\tilde{\kappa}_s + \tau s_l^{(0)}\right) s_l^{(0)2} \quad \text{on} \quad \Gamma_p, \tag{4.74}$$

$$s_g^{(2)} \text{ is periodic} \quad \text{on} \quad \partial\omega, \tag{4.75}$$

where we have used (4.60) to simplify (4.73).

Integrating (4.71) and (4.72) over $\omega_g^{(0)}$ and $\omega_l^{(0)}$, respectively, and applying first the Divergence Theorem and then Leibniz' Rule together with periodicity of $s_g^{(1)}$ and

$s_g^{(2)}$ we obtain

$$\tau\eta\mathcal{V}_g\frac{\partial s_g^{(0)}}{\partial t} = \nabla_X\cdot\left(\mathcal{V}_g\left(\mathbf{I}+\frac{1}{\mathcal{V}_g}\iiint_{\omega_g^{(0)}}\nabla_x\boldsymbol{\Omega}\,\mathrm{d}V\right)\nabla_X s_g^{(0)}\right)$$

$$+\iint_{\Gamma_i^{(0)}}\nabla_X a^{(0)}\cdot\left(\nabla_x s_g^{(1)}+\nabla_X s_g^{(0)}\right)-\left(\nabla_X s_g^{(1)}+\nabla_x s_g^{(2)}\right)\cdot\boldsymbol{e}_r\,\mathrm{d}S, \tag{4.76}$$

$$\tau\mathcal{V}_l\frac{\partial s_l^{(0)}}{\partial t} = \nabla_X\cdot\left(\mathcal{V}_l\left(\mathbf{I}+\frac{1}{\mathcal{V}_l}\iiint_{\omega_l^{(0)}}\nabla_x\boldsymbol{\Theta}\,\mathrm{d}V\right)\nabla_X s_l^{(0)}\right)$$

$$-\iint_{\Gamma_i^{(0)}}\nabla_X a^{(0)}\cdot\left(\nabla_x s_l^{(1)}+\nabla_X s_l^{(0)}\right)+\left(\nabla_X s_l^{(1)}+\nabla_x s_l^{(2)}\right)\cdot\boldsymbol{e}_r\,\mathrm{d}S$$

$$-\iint_{\Gamma_p}\left(\nabla_X s_l^{(1)}+\nabla_x s_l^{(2)}\right)\cdot\boldsymbol{e}_r\,\mathrm{d}S, \tag{4.77}$$

where $\mathcal{V}_l = 1-\mathcal{V}_g-4\pi\lambda^3/3$ is the volume of the liquid phase. We now multiply (4.77) by σ_s, combine with (4.76), and use the boundary conditions (4.73) and (4.74) together with (4.56) to obtain the macroscale equations that govern the evolution of $s_g^{(0)}$ and $a^{(0)}$ which, dropping the superscripts, read

$$\tau\frac{\partial s_g}{\partial t} = \frac{1}{\mathcal{V}_1}\nabla_X\cdot(\mathcal{V}_2\mathbf{D}\nabla_X s_g)-\frac{2\sigma_s\left(\tilde{\kappa}_s+\tau s_g\right)s_g^2\mathcal{S}_{gl}}{\mathcal{V}_1\left(1+a/\lambda\right)^2}, \tag{4.78}$$

$$\frac{\partial a}{\partial t} = \frac{2s_g^2}{(1+a/\lambda)^2}, \tag{4.79}$$

where

$$\mathbf{D}_{ij} = \delta_{ij}+\frac{1}{\mathcal{V}_2}\left(\iiint_{\omega_g}\frac{\partial\Omega_j}{\partial x_i}\,\mathrm{d}V+\sigma_s\iiint_{\omega_l}\frac{\partial\Theta_j}{\partial x_i}\,\mathrm{d}V\right), \tag{4.80}$$

$$\mathcal{V}_1 = \eta\mathcal{V}_g+\sigma_s\mathcal{V}_l,\qquad \mathcal{V}_2 = \mathcal{V}_g+\sigma_s\mathcal{V}_l. \tag{4.81}$$

In this limit, since the mass transfer of sulphur dioxide between the gas and the liquid phase is $O(1)$, we must solve two cell problems, and the diffusivity tensor takes account of the diffusivities in both the gas and the liquid domain (unlike the previous limit, which only depended on the diffusivity in the gas domain).

4.3. Uniformly Valid Equations. We combine the results from the limits in Subsections 4.1 and 4.2 into a uniformly valid set of macroscale equations to obtain

$$\tau\frac{\partial s_g}{\partial t} = \frac{1}{\mathcal{V}_1}\nabla_X\cdot(\mathcal{V}_2\mathbf{D}\nabla_X s_g)-\frac{2\sigma_s\left(\kappa_s/\epsilon^2+\tau s_g\right)\left(s_l^{(0)}|_{r=\lambda}\right)^2\mathcal{S}_{gl}}{\mathcal{V}_1\left(1+a/\lambda\right)^2}, \tag{4.82}$$

$$\frac{\partial a}{\partial t} = \frac{2\left(s_l^{(0)}|_{r=\lambda}\right)^2}{(1+a/\lambda)^2}, \tag{4.83}$$

where $s_l^{(0)}|_{r=\lambda}$, $\mathbf{D}$, $\mathcal{V}_1$, and $\mathcal{V}_2$ are defined as in (4.25), (4.80), and (4.81), respectively. Setting either σ_s or κ_s to be $O(\epsilon^2)$ recovers the previous limits, while further simplifications can be made if both $\sigma_s,\kappa_s\ll 1$.

4.4. A Comment on the Limit When $\sigma_s, \kappa_s = O(1)$. In this limit, sulphur dioxide will be depleted at a much faster rate than in the previous two limits. The leading-order governing equations for $s_g^{(0)}$ and $s_l^{(0)}$ in this case are

$$\nabla_x^2 s_g^{(0)} = 0 \qquad \text{in} \qquad \omega_g^{(0)}, \tag{4.84}$$

$$\nabla_x^2 s_l^{(0)} = 0 \qquad \text{in} \qquad \omega_l^{(0)}, \tag{4.85}$$

subject to the boundary conditions

$$\nabla_x s_l^{(0)} \cdot \boldsymbol{e}_r = 2\kappa_s s_l^{(0)2} \qquad \text{on} \qquad \Gamma_p, \tag{4.86}$$

$$-\nabla_x s_g^{(0)} \cdot \boldsymbol{e}_r = -\sigma_s \nabla_x s_l^{(0)} \cdot \boldsymbol{e}_r \qquad \text{on} \qquad \Gamma_i^{(0)}, \tag{4.87}$$

$$s_g^{(0)} = s_l^{(0)} \qquad \text{on} \qquad \Gamma_i^{(0)}, \tag{4.88}$$

$$s_g^{(0)} \text{ is periodic} \qquad \text{on} \qquad \partial\omega. \tag{4.89}$$

Applying the Divergence Theorem to (4.84) and (4.85), and using (4.86), (4.87), and (4.89), we conclude that

$$s_l^{(0)} = 0 \qquad \text{on} \qquad \Gamma_p. \tag{4.90}$$

Then, solving (4.85), with (4.86), (4.90) and the radial symmetry of $s_l^{(0)}$, we obtain

$$s_l^{(0)} = 0 \qquad \text{in} \qquad \omega_l^{(0)}. \tag{4.91}$$

Following the previous arguments in (4.22)–(4.24) (where (4.87) and (4.91) reduce to (4.15)), we see that $s_g^{(0)}$ is independent of the microscale variables and, thus, using (4.88), we establish that

$$s_g^{(0)} = 0 \qquad \text{in} \qquad \omega_g^{(0)}, \tag{4.92}$$

i.e., all the sulphur dioxide is consumed. This suggests that, in this case, sulphur dioxide consumption happens on a faster timescale than the liquid-layer-growth timescale we have used to non-dimensionalise the model, and, in fact, we need to rescale time by ϵ^2 so that the time derivative in (4.85) enters the leading-order equation for $s_l^{(0)}$. As in [14], in this regime, there is a limit in which $\eta = O(\epsilon^2)$, which simplifies the leading-order version of (4.3), but retains the time derivative in the leading-order version of (4.4). However, unlike in [14], the resulting equations cannot be solved explicitly due to the non-linearity in the boundary conditions on the surface of the catalytic pellet and the moving boundary that is present.

We note that we obtain the same conclusions if we assume $\sigma_s\kappa_s = O(\epsilon)$ and one of κ_s or σ_s is $O(1)$. In these limits, the combined effect of the mass transfer and reaction is strong enough to consume all the sulphur dioxide to leading order on our chosen timescale.

4.5. Physically Relevant Limit. It is clear that the limits in which $\sigma_s\kappa_s = O(\epsilon^2)$ provide the largest values of the parameters for which we obtain non-trivial solutions for the sulphur dioxide concentration on our timescale. Furthermore, the values of the physical parameters also suggest that these are the physically relevant regimes, since otherwise the device would fill with liquid and lose efficiency much faster than the experiments indicate. In fact, using actual parameter values, the most

relevant limit is $\kappa_s, \sigma_s = O(\epsilon)$. This is a sub-limit of the other two considered in Subsection 4.1 and 4.2, and the governing equations in this case can be obtained, for example, by letting $\kappa_s \to 0$ in (4.42) and (4.43) or using the equations in Subsection 4.3 with $\kappa_s, \sigma_s = O(\epsilon)$. Writing $\kappa_s = \epsilon\bar{\kappa}_s, \sigma_s = \epsilon\bar{\sigma}_s$, where $\bar{\kappa}_s, \bar{\sigma}_s = O(1)$, we find that

$$\tau\eta\frac{\partial s_g}{\partial t} = \frac{1}{\mathcal{V}_g}\nabla_X \cdot (\mathcal{V}_g D \nabla_X s_g) - \frac{2\bar{\sigma}_s\bar{\kappa}_s\mathcal{S}_{gl}s_g^2}{\mathcal{V}_g\left(1+a/\lambda\right)^2}, \tag{4.93}$$

$$\frac{\partial a}{\partial t} = \frac{2s_g^2}{(1+a/\lambda)^2}, \tag{4.94}$$

where D, $\mathcal{V}_g$, and $\mathcal{S}_{gl}$ are as defined in (4.44) and (4.45), respectively.

5. Device-Scale Model. Now that we have derived the macroscale equations for the sulphur dioxide concentration and the thickness of the liquid acid layer within the filter sheets, we need to incorporate these in a model for the whole device. We consider the filter as shown on the left in Figure 1, which we reproduce with the relevant coordinate system (with macroscale variables $\hat{X}, \hat{Y}, \hat{Z}$) and length scales in Figure 4. The flue gas flows up through a channel of half-width d and length L alongside a filter sheet of thickness H, width W, and length L. In the filter channel, since the gas flow is uniform in the $\hat{Z}$-direction and we assume no flux of gas at $\hat{Y} = \pm W/2$, we anticipate negligible variation in the $\hat{X}$-direction and no variation in the $\hat{Y}$-direction. We note that, on the surface of the filter sheet, we could have applied the boundary condition found in Beavers and Joseph [3] to account for the transmission of longitudinal flow from the channel into the porous medium. This would introduce a thin layer, near the surface, across which the gas velocity is reduced to zero. Since our focus is on the generation of liquid inside the filter sheet, for simplicity we assume the channel wall provides no retardation to the flow. Thus, conservation of mass of sulphur dioxide with cross-sectionally averaged concentration $\hat{S}(\hat{z}, \hat{t})$ reads

$$d\left(\frac{\partial \hat{S}}{\partial \hat{t}} + U\frac{\partial \hat{S}}{\partial \hat{Z}}\right) = \left[\frac{\hat{\mathcal{V}}_g\left(\hat{a}\right)}{l^3}\hat{D}(\hat{a})\frac{\partial \hat{s}_g}{\partial \hat{X}}\right]_{\hat{X}=d}, \tag{5.1}$$

where U is the constant speed of the gas flow, $\hat{\mathcal{V}}_g\left(\hat{a}\right)/l^3 = \mathcal{V}_g$ is the void fraction in the filter sheets (defined in (4.45)), and $\hat{D}(\hat{a}) = D_{s_g}D(a)$ with D defined in (4.44). The right-hand side of (5.1) accounts for the uptake of sulphur dioxide by the filter device at $\hat{X} = d$, while we have assumed zero flux at $\hat{X} = 0$ and $\hat{Y} = \pm W/2$. We note that we have neglected diffusion along the channel, which is justifiable, since the Péclet number $\mathrm{Pe} = UL/D_{s_g} = 10^4 \gg 1$. In the filter sheet, we track the concentration, $\hat{s}_g$, of sulphur dioxide and the void fraction $\mathcal{V}_g$. The dimensional forms of (4.93) and (4.94), in which we have replaced $\hat{a}$ with $\hat{\mathcal{V}}_g$ using the dimensional form of (4.45), read

$$\frac{\partial \hat{s}_g}{\partial \hat{t}} = \frac{1}{\hat{\mathcal{V}}_g}\nabla_{\hat{X}} \cdot \left(\hat{\mathcal{V}}_g\hat{D}\nabla_{\hat{X}}\hat{s}_g\right) - \left(\frac{8\pi R^2 k}{\beta_s^2}\right)\frac{\hat{s}_g^2}{\hat{\mathcal{V}}_g}, \tag{5.2}$$

$$\frac{\partial \hat{\mathcal{V}}_g}{\partial \hat{t}} = -\left(\frac{8\pi V_m R^2 k}{\beta_s^2}\right)\hat{s}_g^2. \tag{5.3}$$

At the surface of the sheet, we assume that the concentration is continuous, and so we write

$$\hat{s}_g = \hat{S} \qquad \text{at} \qquad \hat{X} = d. \tag{5.4}$$

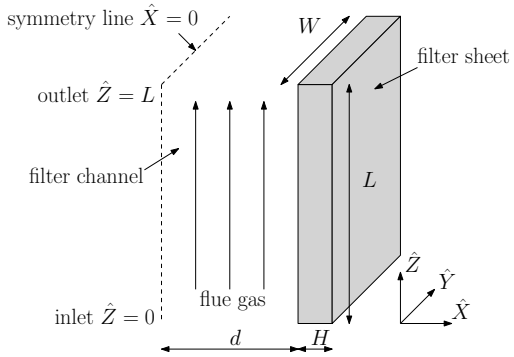

FIGURE 4. *Schematic of the filter.*

We note that the void fraction does not appear in (5.4), since $\hat{s}_g$ is the concentration of sulphur dioxide averaged over the gas phase and not the whole space. At the back of the filter sheet, we assume that no sulphur dioxide can escape and write

$$\frac{\partial \hat{s}_g}{\partial \hat{X}} = 0 \qquad \text{at} \qquad \hat{X} = d + H. \tag{5.5}$$

At the inlet of the filter, both the channels and the filter sheets are exposed to the incoming gas stream. We assume that sulphur dioxide of constant concentration S_0 is supplied to the filter

$$\hat{s}_g = \hat{S} = S_0 \qquad \text{at} \qquad \hat{Z} = 0. \tag{5.6}$$

At the bottom of the sheet, the filter is open, and, thus, we assume that the two concentrations are the same, and so we have that

$$\hat{s}_g = \hat{S} \qquad \text{at} \qquad \hat{Z} = L. \tag{5.7}$$

At the two ends along the width of the sheet, we assume no flux of sulphur dioxide

$$\frac{\partial \hat{s}_g}{\partial \hat{Y}} = 0 \qquad \text{at} \qquad \hat{Y} = \pm\frac{W}{2}. \tag{5.8}$$

Finally, we assume no sulphur dioxide or liquid sulphuric acid are initially present in the filter; these conditions read

$$\hat{s}_g = \hat{S} = 0, \qquad \hat{\mathcal{V}}_g = l^3 - \frac{4}{3}\pi R^3 \qquad \text{at} \qquad \hat{t} = 0, \tag{5.9}$$

We non-dimensionalise (5.1)–(5.9) using

$$\begin{gathered} \hat{X} = d + HX, \quad \hat{Y} = WY, \quad \hat{Z} = LZ, \quad \hat{t} = (L^2/D_{s_g})t, \\ \hat{S} = S_0 S, \quad \hat{\mathcal{V}}_g = l^3 \mathcal{V}_g, \quad \hat{D} = D_{s_g} D, \end{gathered} \tag{5.10}$$

where we have picked the timescale based on diffusion along the length of the filter sheet. We note that the diffusive timescale in the transverse, X, direction is much smaller than this timescale and not of particular interest with regards to the long-term operation of the device. In addition, since the flue gas flows uniformly along

the channel, and we prescribe zero flux of sulphur dioxide at $Y = \pm 1/2$, there are no variations in the Y-direction of s_g or S. The dimensionless equations are

$$\delta\varepsilon\left(\frac{\partial S}{\partial t} + \mathrm{Pe}\frac{\partial S}{\partial Z}\right) = \left(\mathcal{V}_g D\frac{\partial s_g}{\partial X}\right)\Bigg|_{X=0}, \tag{5.11}$$

$$\delta^2\frac{\partial s_g}{\partial t} = \frac{1}{\mathcal{V}_g}\left(\frac{\partial}{\partial X}\left(\mathcal{V}_g D\frac{\partial s_g}{\partial X}\right) + \delta^2\frac{\partial}{\partial Z}\left(\mathcal{V}_g D\frac{\partial s_g}{\partial Z}\right)\right) - \frac{\delta^2\Upsilon s_g^2}{\alpha\mathcal{V}_g}, \tag{5.12}$$

$$\frac{\partial \mathcal{V}_g}{\partial t} = -\Upsilon s_g^2, \tag{5.13}$$

subject to

$$s_g = S \quad \text{at} \quad X = 0, \tag{5.14}$$

$$\frac{\partial s_g}{\partial X} = 0 \quad \text{at} \quad X = 1, \tag{5.15}$$

$$s_g = S = 1 \quad \text{at} \quad Z = 0, \tag{5.16}$$

$$s_g = S \quad \text{at} \quad Z = 1, \tag{5.17}$$

$$s_g = S = 0 \quad \text{at} \quad t = 0, \tag{5.18}$$

$$\mathcal{V}_g = 1 - \frac{4\pi\lambda^3}{3} \quad \text{at} \quad t = 0, \tag{5.19}$$

where we have the following six dimensionless parameters with corresponding orders of magnitude

$$\begin{gathered}\alpha = V_m S_0 \approx 10^{-6}, \quad \delta = \frac{H}{L} \approx 10^{-2}, \quad \varepsilon = \frac{d}{L} \approx 10^{-2}, \quad \lambda = \frac{R}{l} \approx 10^{-1}, \\ \Upsilon = \frac{8\pi V_m R^2 k L^2 S_0^2}{\beta_s^2 l^3 D_{s_g}} \approx 10^{-1}, \quad \mathrm{Pe} = \frac{LU}{D_{s_g}} \approx 10^4.\end{gathered} \tag{5.20}$$

Here, α measures the change in volume in the gas-to-liquid transition in the chemical reaction, δ is the aspect ratio of the filter sheet, ε is the aspect ratio of the filter channel, λ is the ratio of the catalytic pellet radius to the inter-pellet distance (as introduced in (3.11)), Υ is a ratio of the diffusive timescale to the timescale over which the liquid layer grows, and Pe is the Péclet number.

6. Asymptotic Results for a Slender Filter Device. As seen in (5.20), $\delta \ll 1$. Furthermore, under normal operating conditions, the gas flow is advection-dominated, so that $\mathrm{Pe} \gg 1$. We exploit these facts to further simplify the system of equations presented in the previous section. In particular, we systematically explore two physically relevant distinguished limits by varying α and ε which control the system behaviour. In all the limits, based on experimental evidence, we assume $\mathrm{Pe} = O(1/\delta^2)$ and, for the richest asymptotic limit, we assume $\Upsilon = O(1)$.

6.1. Limit I: $\alpha = O(\delta^2)$ and $\varepsilon = O(\delta)$. We first study the case when the reaction rate and the diffusive rate are in balance, the channel thickness and sheet thickness are similar, and the concentration of sulphur dioxide supplied at the entrance of the channel is small. We set $\alpha = \delta^2\tilde{\alpha}$, and $\varepsilon = \delta\bar{\varepsilon}$, where $\tilde{\alpha}, \bar{\varepsilon} = O(1)$. Expanding the dependent variables as power series in powers of δ^2, the leading-order versions of

(5.12) and (5.11) become quasi-static, and we find that

$$\bar{\varepsilon}\,\widetilde{\mathrm{Pe}}\frac{\partial S}{\partial Z} = \left(\mathcal{V}_g D\frac{\partial s_g}{\partial X}\right)\Bigg|_{X=0}, \tag{6.1}$$

$$0 = \frac{1}{\mathcal{V}_g}\left(\frac{\partial}{\partial X}\left(\mathcal{V}_g D\frac{\partial s_g}{\partial X}\right)\right) - \frac{\Upsilon s_g^2}{\tilde{\alpha}\mathcal{V}_g}, \tag{6.2}$$

$$\frac{\partial \mathcal{V}_g}{\partial t} = -\Upsilon s_g^2, \tag{6.3}$$

where $\widetilde{\mathrm{Pe}} = \delta^2\mathrm{Pe} = O(1)$. Equations (6.2)–(6.1) must be solved subject to (5.14)–(5.19). We will solve these numerically in Section 7 and will find a monotonically decreasing quasi-static solution for the sulphur dioxide concentration that agrees well with the solution to the full numerical solution as δ decreases.

6.2. Limit II: $\boldsymbol{\alpha = O(\delta)}$ and $\boldsymbol{\varepsilon = O(\delta^2)}$. We now turn our attention to the case when reaction is slower than diffusion, the channel width is much thinner than the sheet width, and there is a moderate amount of sulphur dioxide entering the device. We write $\alpha = \delta\bar{\alpha}$, and $\varepsilon = \delta^2\tilde{\varepsilon}$, where $\bar{\alpha}, \tilde{\varepsilon} = O(1)$. After asymptotically expanding the dependent variables in powers of δ (and dropping the superscripts on the leading-order variables), the leading-order version of (5.12) becomes

$$0 = \frac{1}{\mathcal{V}_g}\left(\frac{\partial}{\partial X}\left(\mathcal{V}_g D\frac{\partial s_g}{\partial X}\right)\right). \tag{6.4}$$

This can be readily integrated, and using (5.15), we obtain

$$s_g = s_g(Z,t). \tag{6.5}$$

The $O(\delta)$ versions of (5.11) and (5.12) read

$$\tilde{\varepsilon}\,\widetilde{\mathrm{Pe}}\frac{\partial S}{\partial Z} = \left(\mathcal{V}_g D\frac{\partial s_g^{(1)}}{\partial X}\right)\Bigg|_{X=0}. \tag{6.6}$$

$$0 = \frac{1}{\mathcal{V}_g}\frac{\partial}{\partial X}\left(\mathcal{V}_g D\frac{\partial s_g^{(1)}}{\partial X}\right) - \frac{\Upsilon s_g^2}{\bar{\alpha}\mathcal{V}_g}, \tag{6.7}$$

Multiplying (6.7) by $\mathcal{V}_g$ and integrating it with respect to X from 0 to 1, and using (5.14), (5.15) and (6.6) we obtain

$$0 = -\frac{\Upsilon}{\bar{\alpha}}S^2 - \tilde{\varepsilon}\,\widetilde{\mathrm{Pe}}\frac{\partial S}{\partial Z}, \tag{6.8}$$

which we solve alongside

$$\frac{\partial \mathcal{V}_g}{\partial t} = -\Upsilon S^2, \tag{6.9}$$

together with the conditions

$$S = 1 \qquad \text{at} \qquad Z = 0, \tag{6.10}$$

$$\mathcal{V}_g = 1 - \frac{4\pi\lambda^3}{3} \qquad \text{at} \qquad t = 0. \tag{6.11}$$

Writing $\beta = \Upsilon/\bar{\alpha}\,\bar{\varepsilon}\,\widetilde{\mathrm{Pe}}$, the solution is

$$S = \frac{1}{1+\beta Z}, \qquad \mathcal{V}_g = 1 - \frac{4\pi\lambda^3}{3} - \frac{\Upsilon t}{(1+\beta Z)^2} \tag{6.12}$$

In this limit, we see that S has reached a steady state, while $\mathcal{V}_g$ evolves linearly in time. Furthermore, using (6.12), we can calculate the first time when liquid layers around the pellets adjacent to the inlet of the channel touch each other, after which moment we will need a different model to account for the coalescence. The critical void fraction at which this happens is $\mathcal{V}_{g,c} = 1 - \pi/6$ (the largest sphere that can fit in the unit cube has radius $\pi/6$), and, therefore, using (6.12) evaluated at $Z = 0$, the asymptotic value of the critical time t_c^a is calculated to be

$$t_c^a = \frac{\pi}{6\Upsilon}\left(1 - 8\lambda^3\right). \tag{6.13}$$

7. Numerical Results. We solve (5.12)–(5.19) numerically using a second-order-accurate finite-difference scheme, implemented in MATLAB. In Figure 5, we show plots of the spatial profiles of S in the channel and $\mathcal{V}_g$ at the edge of the filter at $X = 0$ for various times (the parameter values are shown in the figure caption). We stop the simulations at the time when two neighbouring liquid layers adjacent to the inlet of the channel coalesce ($t_c \approx 0.52$ in this simulation). After this point, our model becomes unphysical, and we would need to consider transport through a fully flooded microstructure, but this is beyond the scope of this paper. We see that, as time increases, the concentration of sulphur dioxide increases and approaches a quasi-steady state, which can be more easily seen in Figure 6 (left), where we plot a temporal profile of S at the outlet of the channel $Z = 1$. In Figure 6 (left), we can also see the breakthrough curve that describes the steep increase in the concentration of sulphur dioxide and the point in time when the gas initially fills up the channel. The slow increase in concentration at the end of the channel is due to the gradual accumulation of liquid sulphuric acid in the filter sheets. In Figure 5 (right), we see that, as time increases, the void fraction decreases and is smallest near the channel inlet, as expected. In Figure 7, we plot the temporal profile of the ratio, F, of the total amount of sulphur dioxide that has exited the channel at $Z = 1$, compared to the total amount of sulphur dioxide that has entered the channel at $Z = 0$, calculated according to

$$F = \frac{\int_0^t S(1,s)\,\mathrm{d}s}{\int_0^t S(0,s)\,\mathrm{d}s}. \tag{7.1}$$

We see that, similar to Figure 6 (left), F is initially zero until the channel is filled with gas. We also see that F then rises steeply as sulphur dioxide exits the channel then levels off. In Figure 6 (right), we show spatial profiles of S and $\mathcal{V}_g$ in the filter sheet at the middle of the channel at $t = t_c$. As anticipated, the concentration of sulphur dioxide decreases deeper into the sheet, and the void fraction increases.

In Figure 8, we show the temporal evolution of S at the channel outlet $Z = 1$ as we vary four of the dimensionless parameters, namely $\alpha, \varepsilon, \Upsilon$ and Pe. We see that decreasing α decreases the concentration of sulphur dioxide at the outlet, since this corresponds to lower amounts of sulphur dioxide being fed into the device. However, increasing ε increases the concentration, since this corresponds to wider channels, which contain more sulphur dioxide. Increasing Υ, though, decreases the critical time

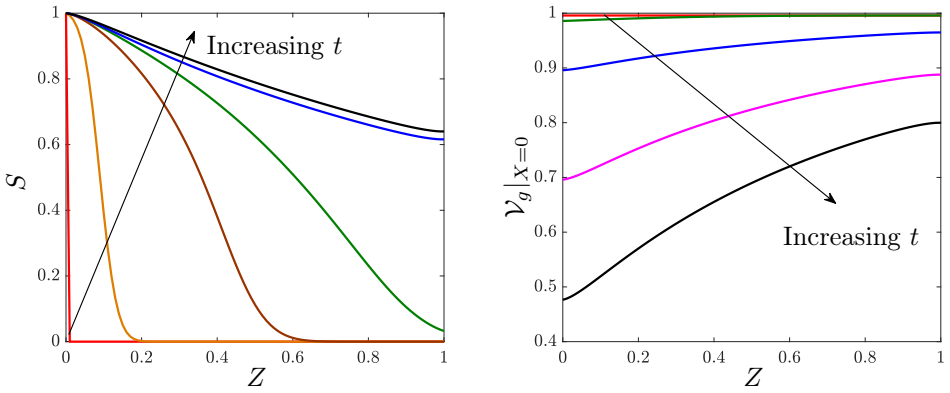

FIGURE 5. *(Left) Spatial profile of S in the channel at $t = 0.52$ and (right) $\mathcal{V}_g$ on the channel wall at $X = 0$ for various times t: 0 (red), 0.001 (orange), 0.005 (brown), 0.01 (green), 0.1 (blue), 0.3 (magenta), 0.52 (black). In these plots, $\delta = 0.1, \varepsilon = 0.1, \Upsilon = 1, \mathrm{Pe} = 100, \alpha = 0.01, \lambda = 0.1$.*

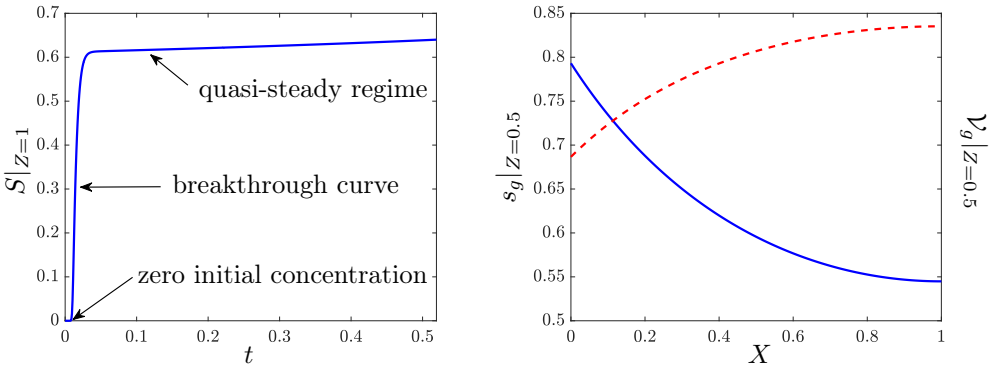

FIGURE 6. *(Left) Temporal profile of S at the outlet of the channel $Z = 1$. (Right) Spatial profiles of s_g (blue) and $\mathcal{V}_g$ (dashed red) in the sheet at the middle of the channel $Z = 0.5$. In these plots, $\delta = 0.1, \varepsilon = 0.1, \Upsilon = 1, \mathrm{Pe} = 100, \alpha = 0.01, \lambda = 0.1$.*

for liquid coalescence, t_c, and the sulphur dioxide concentration, which is expected, as this corresponds to increasing the reaction rate k. Increasing Pe increases the concentration, as this corresponds to increasing the speed of the gas. Furthermore, in Figure 9, we show the temporal profile of F for different values of Pe. We see that increasing Pe increases F and thus decreases the efficiency of the filter. Thus, we can use these results to calculate the maximum flow speed of the gas in order to remove a given proportion of the incoming sulphur dioxide, or keep the outlet concentration of sulphur dioxide below a given threshold. We note that we have used a different set of base parameter values for δ and Pe than in (5.20), since the simulations become computationally challenging in this case. The aim here is to illustrate the general qualitative behaviour of the system, and then to use asymptotic reductions (when $\delta \ll 1$), thus enabling a quicker solution.

In Figure 10, we show spatial profiles of the numerical solution to (5.12)–(5.19) for decreasing δ compared to the solution of the asymptotically reduced equations (6.2)–(6.1) and the asymptotic result (6.12), respectively. When we vary δ, we also vary α and ε according to the limits considered in Subsections 6.1 and 6.2, respectively. We

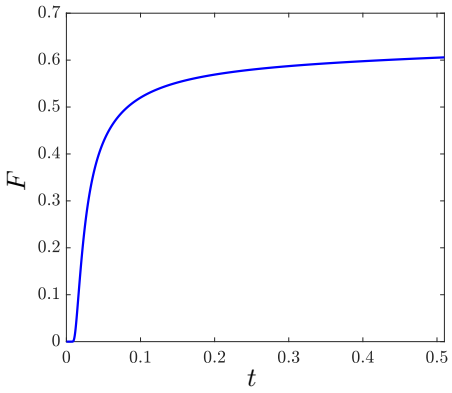

FIGURE 7. *Temporal profile of the ratio, F, of the total amount of sulphur dioxide that has exited the channel at $Z = 1$, compared to the total amount of sulphur dioxide that has entered the channel at $Z = 0$. In this plot, $\delta = 0.1, \varepsilon = 0.1, \Upsilon = 1, \mathrm{Pe} = 100, \alpha = 0.01, \lambda = 0.1$.*

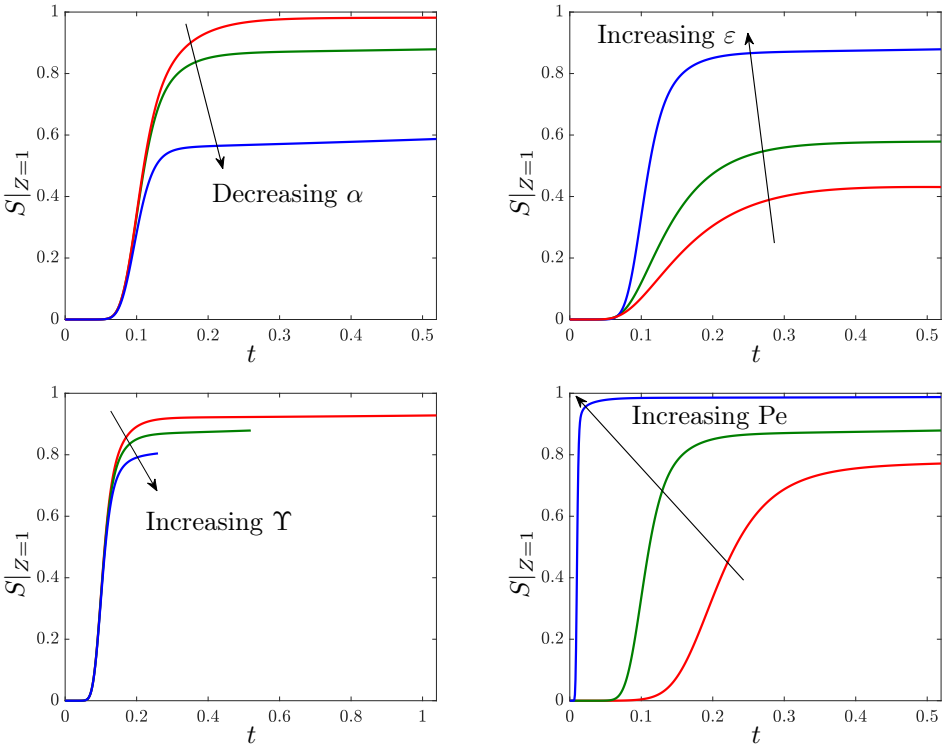

FIGURE 8. *Plots of the temporal profile of S at the channel outlet $Z = 1$ varying (top left) $\alpha = 1$ (red), 0.1 (green), and 0.01 (blue) keeping $\varepsilon = 1, \Upsilon = 1, \mathrm{Pe} = 10$, (top right) $\varepsilon = 0.1$ (red), 0.2 (green), and 1 (blue) keeping $\alpha = 0.1, \Upsilon = 1, \mathrm{Pe} = 10$, (bottom left) $\Upsilon = 0.5$ (red), 1 (green), and 2 (blue) keeping $\alpha = 0.1, \varepsilon = 1, \mathrm{Pe} = 10$, and (bottom right) $\mathrm{Pe} = 5$ (red), 10 (green), and 100 (blue) keeping $\alpha = 0.1, \varepsilon = 1, \Upsilon = 1$. In these plots, $\delta = 0.3, \lambda = 0.1$.*

see a very good agreement even at moderate values of δ, noting that the convergence in Figure 10 (right) is slower. We note that, in order to obtain the asymptotic results

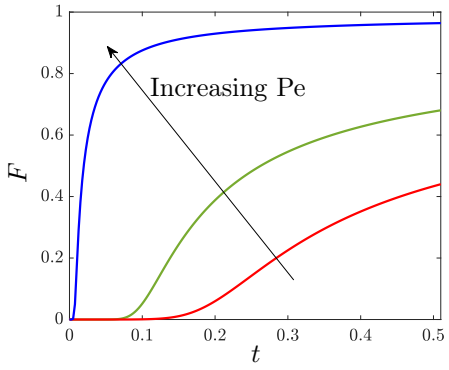

FIGURE 9. *Temporal profile of the ratio, F, of the total amount of sulphur dioxide that has exited the channel, compared to the total amount of sulphur dioxide that has entered the channel, varying* $\mathrm{Pe} = 5$ *(red),* 10 *(green), and* 100 *(blue) keeping* $\alpha = 0.1, \varepsilon = 1, \Upsilon = 1$, $\delta = 0.3, \lambda = 0.1$.

in Figure 10 (left), we start the numerical simulation with the early-time asymptotic solution of (5.12)–(5.19) when $t = O(\delta^2)$.

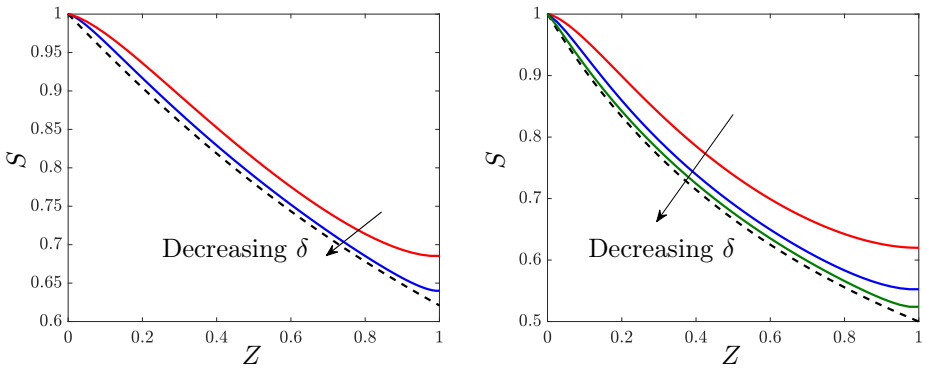

FIGURE 10. *Plots of the spatial profile of S at $t = 0.52$ for (left) $\delta = 0.3$ (red), $\delta = 0.1$ (blue), and the corresponding asymptotic results in Subsection 6.1 and for (right) $\delta = 0.3$ (red), $\delta = 0.1$ (blue), $\delta = 0.03$ (green) and the corresponding asymptotic results in Subsection 6.2 (dashed black).*

8. Discussion and Conclusions. In this paper, we developed a mathematical model to describe the operation of a device that converts gaseous sulphur dioxide into liquid sulphuric acid through a chemical reaction that occurs on the surface of catalytic beads contained in a filter. Our aim was to track the spatial and temporal evolution of the concentration of sulphur dioxide and the local amount of acid in the filter along with the concentration of sulphur dioxide in the gas to be purified. Furthermore, we assumed that other chemical species (oxygen and water vapour) participating in the reaction are abundant in the system and, hence, of constant concentration. We began by describing the model that holds on the scale of a single catalytic pellet in the filter sheets, around which a uniform layer of liquid sulphuric acid forms. We then systematically homogenised these equations and derived a set of macroscale equations that describe the whole filter that captures the effect of the porous microstructure via (i) an effective "sink" term in the macroscale equation for the concentration of sulphur

dioxide in the filter, and (ii) an effective diffusivity. We presented two distinguished limits based on the order of magnitude of two dimensionless numbers, κ_s and σ_s, which measure the relative strength of reaction to diffusion and the relative mass transfer on either side of the gas–liquid interface, respectively. In the first limit, when $\kappa_s = O(1)$ and $\sigma_s = O(\epsilon^2)$, the sink term for sulphur dioxide was a complicated non-linear function of the concentration of sulphur dioxide and the thickness of the sulphuric acid. In the second limit, when $\kappa_s = O(\epsilon^2)$ and $\sigma_s = O(1)$, this term simplified considerably but the effective diffusivity became more difficult to calculate. We identified a physically relevant sub-limit, in which both κ_s and σ_s are both small, which simplified the governing equations in the filter sheets.

In the second part of the paper, we coupled the macroscale equations emerging from the homogenisation with a reaction–advection equation for the gas flow in the filter channels between the sheets. We then assumed that the aspect ratio of the filter is small and studied two asymptotic regimes based on the orders of magnitude of two dimensionless numbers, α and ε, which measure the change in volume in the gas-to-liquid transition in the chemical reaction, and the aspect ratio of the channel, respectively. In the first limit, when $\alpha = O(\delta^2)$ and $\varepsilon = O(\delta)$, we obtained a quasi-static equation for the concentration of sulphur dioxide both in the filter sheets and in the channel. In the second limit, when $\alpha = O(\delta)$ and $\varepsilon = O(\delta^2)$, we were able to obtain an explicit solution (6.12) for the concentration of sulphur dioxide and the void fraction. In particular, we found an estimate for the time at which two neighbouring liquid layers around catalytic pellets adjacent to the inlet of the channel will coalesce, which is proportional to the ratio of the timescale over which the liquid layer grows and the diffusive timescale of sulphur dioxide along the channel. From this formula, we see that increasing the inter-pellet distance in the porous sheet increases the time until coalescence, and, thus, increases the device operation time. We solved the full system of macroscale equations numerically and investigated the effect of changing various parameters. Given a target concentration of sulphur dioxide at the outlet, our model can be used to find the maximum speed of the gas that achieves this. We compared the numerical results to our asymptotic predictions and found an excellent agreement and thus, in the relevant limit, the reduced system of equations may be used to approximate the performance of the filter in the given regimes.

Our model captures the initial stage of operation of the filter device before neighbouring liquid layers in the filter sheets coalesce. Once this happens we need to develop another model that accounts for the change in diffusive pathway in the liquid and involves a moving front of liquid inside the filter sheet (see Figure 11). In addi-

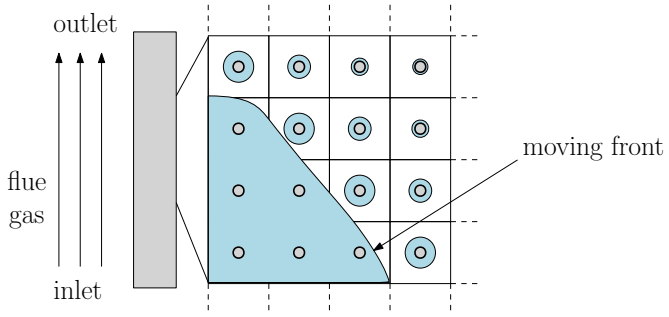

FIGURE 11. *Schematic of a moving liquid-acid front in a porous filter sheet.*

tion, we want to incorporate the effect of the fibre network in the porous sheet, since these fibres can be manufactured to be either hydrophilic or hydrophobic, which may enhance or inhibit the liquid transport within the filter. Our model provides the basis for exploration of the performance of reactive filters and for optimisation in order to minimise the amount of sulphur dioxide released by the device into the atmosphere, while ensuring longevity.

Acknowledgments. This publication is based on work partially supported by the EPSRC Centre For Doctoral Training in Industrially Focused Mathematical Modelling (EP/L015803/1) in collaboration with W. L. Gore and Associates, Inc. We would like to thank U. Beuscher and V. Venkateshwaran from W. L. Gore and Associates, Inc. for their crucial contributions. IMG acknowledges support from the Royal Society via a University Research Fellowship. In compliance with EPSRC's open access initiative, the data in this paper is available from http://doi.org/10.5287/bodleian:KZ8RN2BvO.

REFERENCES

[1] G. Allaire, A. Mikelić, and A. Piatnitski, *Homogenization approach to the dispersion theory for reactive transport through porous media*, SIAM J. Math. Anal., 42 (2010), pp. 125–144, https://doi.org/10.1137/090754935.

[2] G. Allaire and A. Piatnitski, *Homogenization of nonlinear reaction–diffusion equation with a large reaction term*, Ann. Univ. Ferrara, 56 (2010), pp. 141–161, https://doi.org/10.1007/s11565-010-0095-z.

[3] G. S. Beavers and D. D. Joseph, *Boundary conditions at a naturally permeable wall*, J. Fluid Mech., 30 (1967), pp. 19–207, https://doi.org/10.1017/S0022112067001375.

[4] A. Bensoussan, J.-L. Lions, and G. Papanicolaou, *Asymptotic Analysis for Periodic Structures*, North-Holland, 1978.

[5] C. Bringedal, I. Berre, I. S. Pop, and F. A. Radu, *Upscaling of non-isothermal reactive porous media flow with changing porosity*, Transp. Porous Med., 114 (2016), pp. 371–393, https://doi.org/10.1007/s11242-015-0530-9.

[6] C. Bringedal and K. Kumar, *Effective behavior near clogging in upscaled equations for non-isothermal reactive porous media flow*, Transp. Porous Med., 120 (2017), pp. 553–577, https://doi.org/10.1007/s11242-017-0940-y.

[7] T. P. Brown, L. Rushton, M. A. Mugglestone, and D. F. Meechan, *Health effects of a sulphur dioxide air pollution episode*, J. Public Health Med., 25 (2003), pp. 369–371, https://doi.org/10.1093/pubmed/fdg083.

[8] M. Bruna and S. J. Chapman, *Diffusion in spatially varying porous media*, SIAM J. Appl. Math., 75 (2015), pp. 1648–1674, https://doi.org/10.1137/141001834.

[9] Q. Cao and L. Nastac, *Mathematical modelling of slag–metal reactions and desulphurization behaviour in gas-stirred ladle based on the DPM-VOF coupled model*, Ironmaking and Steelmaking, (2019), pp. 1–9, https://doi.org/10.1080/03019233.2019.1629155.

[10] I. L. Chernyavsky, L. Leach, I. L. Dryden, and O. E. Jensen, *Transport in the placenta: Homogenizing haemodynamics in a disordered medium*, Phil. Trans. Soc. A, 369 (2011), pp. 4162–4182, https://doi.org/10.1098/rsta.2011.0170.

[11] C. Conca, J. I. Díaz, A. Liñán, and C. Timofte, *Homogenization in chemical reactive flows*, Electron. J. Differ. Eq., 2004 (2004), pp. 1–22.

[12] M. P. Dalwadi, M. Bruna, and I. M. Griffiths, *A multiscale method to calculate filter blockage*, J. Fluid Mech., 809 (2016), pp. 264–289, https://doi.org/10.1017/jfm.2016.656.

[13] M. P. Dalwadi, I. M. Griffiths, and M. Bruna, *Understanding how porosity gradients can make a better filter using homogenization theory*, Proc. R. Soc. A, 471 (2015), pp. 1–20, https://doi.org/10.1098/rspa.2015.0464.

[14] M. P. Dalwadi, Y. Wang, J. R. King, and N. P. Minton, *Upscaling diffusion through first-order volumetric sinks: a homogenization of bacterial nutrient uptake*, SIAM J. Appl. Math., 78 (2018), pp. 1300–1329, https://doi.org/10.1137/17M1138625.

[15] A. S. Damle, *Modeling of SO_2 Removal in Spray-Dryer Flue-Gas Desulfurization System*, tech. report, 1986, https://doi.org/EPA/600/S7-85/038.

[16] A. Fasano and A. Mikelić, *On the filtration through porous media with partially soluble*

permeable grains, Nonlinear Differ. Equ. Appl., 7 (2000), pp. 91–105, https://doi.org/10.1007/PL00001424.

[17] V. E. Fioletov, C. A. McLinden, N. Krotkov, C. Li, J. Joiner, N. Theys, S. Carn, and M. D. Moran, *A global catalogue of large SO_2 sources and emissions derived from the Ozone Monitoring Instrument*, Atmos. Chem. Phys., 16 (2016), pp. 11497–11519, https://doi.org/10.5194/acp-16-11497-2016.

[18] M. Gahn, M. Neuss-Radu, and P. Knabner, *Homogenization of reaction–diffusion processes in a two-component porous medium with nonlinear flux conditions at the interface*, SIAM J. Appl. Math., 76 (2016), pp. 1819–1843, https://doi.org/10.1137/15M1018484.

[19] V. Gaur, R. Asthana, and N. Verma, *Removal of SO_2 by activated carbon fibers in the presence of O_2 and H_2O*, Carbon, 44 (2006), pp. 46–60, https://doi.org/10.1016/j.carbon.2005.07.012.

[20] V. M. H. Govindarao and K. V. Gopalakrishna, *Oxidation of sulfur dioxide in aqueous suspensions of activated carbon*, Ind. Chem. Eng. Res., 34 (1995), pp. 2258–2271, https://doi.org/10.1021/ie00046a007.

[21] S. M. Hashemi, A. Mehrabani-Zeinabad, M. H. Zare, and S. Shirazian, *SO_2 removal from gas streams by ammonia scrubbing: process optimization by response surface methodology*, Chem. Eng. Technol., 42 (2019), pp. 45–52, https://doi.org/10.1002/ceat.201800352.

[22] U. Hornung, *Homogenization and Porous Media*, Springer, 1997.

[23] X. Jiang, Y. Liu, and M. Gu, *Absorption of sulphur dioxide with sodium citrate buffer solution in a rotating packed bed*, Chinese J. Chem. Eng., 19 (2011), pp. 687–692, https://doi.org/10.1016/S1004-9541(11)60042-6.

[24] S. Kiil, M. L. Michelsen, and K. Dam-Johansen, *Experimental investigation and modeling of a wet flue gas desulfurization pilot plant*, Ind. Chem. Eng. Res., 37 (1998), pp. 2792–2806, https://doi.org/10.1021/ie9709446.

[25] R. Klaassen, *Achieving flue gas desulphurization with membrane gas absorption*, Filtration and Separation, 40 (2003), pp. 26–28, https://doi.org/10.1016/S0015-1882(03)00033-8.

[26] J. Knotts and K. Gueniou, *A complete mercury control system*, tech. report, 2017, https://doi.org/IEEE-IAS/PCA.

[27] D. Landa-Marbán, G. Bødtker, K. Kumar, I. S. Pop, and F. A. Radu, *An upscaled model for permeable biofilm in a thin channel and tube*, Transp. Porous. Med., 132 (2020), pp. 83–112, https://doi.org/10.1007/s11242-020-01381-5.

[28] D. G. Leaist, *Diffusion coefficient of aqueous sulfur dioxide at 25 °C*, J. Chem. Eng. Data, 29 (1984), pp. 281–282, https://doi.org/doi.org/10.1021/je00037a015.

[29] E. Luckins, C. J. W. Breward, I. M. Griffiths, and Z. Wilmott, *Homogenisation problems in reactive decontamination*, Eur. J. Appl. Math., (2019). To appear.

[30] W. J. Massman, *A review of the molecular diffusivities of H_2O, CO_2, CH_4, CO, O_3, SO_2, NH_3, N_2O, NO, and NO_2 in air, O_2 and N_2 near STP*, Atmos. Environ., 32 (1998), pp. 1111–1127, https://doi.org/10.1016/S1352-2310(97)00391-9.

[31] S. A. Meier, M. A. Peter, and M. Böhm, *A two-scale modelling approach to reaction-diffusion processes in porous materials*, Comput. Mater. Sci., 39 (2007), pp. 29–34, https://doi.org/10.1016/j.commatsci.2006.02.017.

[32] J. A. Michalski, *Equilibria in a limestone based FGD process: a pure system and with chloride addition*, Chem. Eng. Technol., 24 (2001), p. 1059, https://doi.org/10.1002/1521-4125(200110)24:10<1059::AID-CEAT1059>3.0.CO;2-3.

[33] I. Mochida, K. Kuroda, S. Kawano, Y. Matsumura, M. Yoshikawa, E. Grulke, and R. Andrews, *Kinetic study of the continuous removal of SO_x using polyacrylonitrile-based activated carbon fibres: 2. Kinetic model*, Fuel, 76 (1997), pp. 537–541, https://doi.org/10.1016/S0016-2361(97)00020-3.

[34] R. H. Perry and D. W. Green, *Perry's Chemical Engineers' Handbook*, 1997, https://doi.org/10.5860/choice.38-0966.

[35] N. Peschen, *Conversion of a wet-process flue-gas desulfurization plant from quicklime (CaO) to chalk ($CaCO_3$)*, Chem. Eng. Technol., 25 (2002), pp. 896–898, https://doi.org/10.1002/1521-4125(20020910)25:9<896::AID-CEAT896>3.0.CO;2-9.

[36] M. Peszynska, A. Trykozko, G. Iltis, and S. Schlueter, *Biofilm growth in porous media: Experiments, computational modeling at the porescale, and upscaling*, Adv. Water Resour., 95 (2016), pp. 288–301, https://doi.org/10.1016/j.advwatres.2015.07.008.

[37] M. A. Peter and M. Böhm, *Multiscale modelling of chemical degradation mechanisms in porous media with evolving microstructure*, Multiscale Model. Sim., 7 (2009), pp. 1643–1668, https://doi.org/10.1137/070706410.

[38] A. Poullikkas, *Review of design, operating, and financial considerations in flue gas desulfurization systems*, Energy Technology & Policy, 2 (2015), pp. 92–103, https://doi.org/10.

1080/23317000.2015.1064794.
[39] Z. Qi and E. L. Cussler, *Microporous hollow fibers for gas absorption: I. Mass transfer in the liquid*, J. Membrane Sci., 23 (1985), pp. 321–332, https://doi.org/10.1016/S0376-7388(00)83149-X.
[40] N. Ray, T. Elbinger, and P. Knabner, *Upscaling the flow and transport in an evolving porous medium with general interaction potentials*, SIAM J. Appl. Math., 75 (2015), pp. 2170–2192, https://doi.org/10.1137/140990292.
[41] N. Ray and R. Schulz, *Derivation of an effective dispersion model for electro-osmotic flow involving free boundaries in a thin strip*, J. Eng. Math., 119 (2019), pp. 167–197, https://doi.org/10.1007/s10665-019-10024-8.
[42] R. Sander, *Compilation of Henry's law constants (version 4.0) for water as solvent*, Atmos. Chem. Phys., 15 (2015), p. 4399–4981, https://doi.org/10.5194/acp-15-4399-2015.
[43] A. Sardar and P. Roy, *SO_2 emission control and finding a way out to produce sulphuric acid from industrial SO_2 emission*, J. Chem. Eng. Process Tech., 6 (2015), https://doi.org/10.4172/2157-7048.1000230.
[44] R. Schulz and P. Knabner, *Derivation and analysis of an effective model for biofilm growth in evolving porous media*, Math. Meth. Appl. Sci., 40 (2017), pp. 2930–2948, https://doi.org/10.1002/mma.4211.
[45] F. J. Valdés-Parada, D. Lasseux, and S. Whitaker, *Diffusion and heterogeneous reaction in porous media: The macroscale model revisited*, Int. J. Chem. React. eng., 15 (2017), https://doi.org/10.1515/ijcre-2017-0151.
[46] T. L. van Noorden, *Crystal precipitation and dissolution in a porous medium: Effective equations and numerical experiments*, Multiscale Model. Simul., 7 (2009), pp. 1220–1236, https://doi.org/10.1137/080722096.
[47] T. L. van Noorden, *Crystal precipitation and dissolution in a thin strip*, Eur. J. Appl. Math., 20 (2009), pp. 69–91, https://doi.org/10.1017/S095679250800765.
[48] T. L. van Noorden, I. S. Pop, A. Ebigbo, and R. Helmig, *An upscaled model for biofilm growth in a thin strip*, Water Resour. Res., 46 (2010), pp. 1–14, https://doi.org/10.1029/2009WR008217.
[49] A. K. Vizhemehr, *Predicting the performance of activated carbon filters at low concentrations using accelerated test data*, PhD thesis, Concordia University, 2014.